Maximum Likelihood Joint Angle and Delay Estimation from Multipath and Multicarrier Transmissions with Application to Indoor Localization over IEEE 802.11ac Radio

Faouzi Bellili, Souheib Ben Amor, Sofiène Affes, *Senior Member, IEEE*,
and Ali Ghrayeb, *Senior Member, IEEE*

Abstract—In this paper, we tackle the problem of joint angle and delays estimation (JADE) of multiple reflections of a known signal impinging on multiple receiving antennae. Based on the importance sampling (IS) concept, we propose a new *non-iterative* maximum likelihood (ML) estimator that enjoys guaranteed global optimality and enhanced high-resolution capabilities for both single- and multi-carrier models. The new ML approach succeeds in transforming the original *multi-dimensional* optimization problem into multiple *two-dimensional* ones thereby resulting in huge computational savings. Moreover, it does not suffer from the off-grid problems that are inherent to most existing JADE techniques. By exploiting the sparsity feature of a carefully designed pseudo-pdf that is intrinsic to the new estimator, we also propose a novel approach that enables the accurate detection of the unknown number of paths over a wide range of practical signal-to-noise ratios (SNRs). Computer simulations show the distinct advantage of the new ML estimator over state-of-the art JADE techniques both in the single- and multi-carrier scenarios. Most remarkably, they suggest that the proposed IS-based ML JADE is statistically efficient as it almost reaches the Camér-Rao lower bound (CRLB) even in the adverse conditions of low SNR levels. Using real-world channel measurements collected from four access points (APs) with IEEE 802.11ac standard's setup parameters in an indoor environment, we also show that the proposed ML estimator achieves a localization performance below 15 cm accuracy.

Index Terms—JADE, AoA estimation, time delay estimation, localization, maximum likelihood, importance sampling, antenna arrays

---

1 INTRODUCTION

IN parametric multipath propagation models, a source signal impinges on an antenna array through a number of rays, each described by an angle-of-arrival (AoA), a time delay (TD), and a path gain. The JADE problem consists then in jointly estimating all the AoAs and their corresponding TDs from a finite number of received samples. The JADE problem arises in many practical situations ranging from military applications (e.g., radar and sonar) to broadband wireless communication systems. Typically, the power to characterize each path with its own angle and delay endows the system with stronger sensorial capabilities leading, for instance, to more robust beamforming techniques [2] and enhanced equalization performance [3]. Moreover, as

- *F. Bellili is with the Department of Electrical and Computer Engineering, University of Manitoba, 75 Chancellor's Circle, Winnipeg, MB R3T 5V6, Canada. E-mail: Faouzi.Bellili@umanitoba.ca.*
- *S. Ben Amor and S. Affes are with the INRS-EMT Research Center, 800 de la Gauchetière Ouest, Bureau 6900, Montreal, QC H5A 1K6, Canada. E-mail: {souheib.ben.amor, affes}@emt.inrs.ca.*
- *A. Ghrayeb is with the Electrical & Computer Engineering Department, Texas A&M University at Qatar, Doha 23874, Qatar. E-mail: ali.ghrayeb@qatar.tamu.edu.*

location-aware services for handhelds are likely to be in high demand for future wireless communication systems, the information about the AoAs and the TDs can be used to design highly-accurate localization techniques [4], [5], [6]. In this context, in order to cope with dense multipath environments, the so-called *fingerprinting* paradigm which recasts source localization into a pattern recognition problem was envisaged in [7], [8], [9]. In particular, it was recently shown that *fingerprinting* with location signatures that are characterized by the AoAs and TDs of each candidate location leads to substantial improvements against location signatures that are characterized by the received signal strength (RSS) [10]. In fact, contrarily to the RSS which varies substantially over a wavelength distance (due to constructive and destructive multipath interference), the AoAs together with the associated TDs form a unique fingerprint for each location [9]. Hence, accurate and low-cost estimation of such multipath parameters can be used along with the *fingerprinting* paradigm to develop very efficient localization algorithms Alternatively, if multiple access points (APs) are available, they can cooperate to localize a mobile user by using the estimated time difference of arrivals (TDOAs) and AoAs (see [12] an [13] for more details). In this paper, we apply for the very first time the IS technique along with the ML concept to the JADE problem over both OFDM and single-carrier transmissions. Roughly speaking, the major difficulty with IS consists in generating multiple (i.e., vector) realizations

according to a given (multi-dimensional) pdf. Much like all the IS-based works mentioned in Section 2, we succeed in designing a separable (i.e., factorable) joint angle-delay *pseudo-pdf* which allows a very easy generation of the required vector realizations. Even more, by exploiting the sparsity of the proposed pseudo-pdf, we derive a simple and yet very accurate approach to estimate the number of paths which is also *a priori* unknown in practice and needs to be estimated even before proceeding to angles and delays acquisition. Computer simulations will show the superiority of the proposed IS-based ML estimator over state-of-the-art ML-type and subspace-based JADE techniques in terms of estimation accuracy, resolution capabilities, and computational complexity. Real-world channel measurements collected using IEEE 802.11ac standard's setup parameters in an indoor environment were also used to investigate the online localization capabilities of the proposed algorithm. Results show a localization performance below 15 cm accuracy.

We organize the rest of this paper as follows: We discuss the related background works in Section 2. In Section 3, we introduce the OFDM system model. In Section 4, we derive the concentrated likelihood function (CLF) of the system whose global maximization is detailed in Section 5. In Section 6, we derive the IS-ML technique in the special case of single-carrier systems. In Section 7, we detail the process of generating the required realizations via the IS concept. In Section 8, we provide the necessary implementation details for the proposed IS-based estimator. In Section 9, we develop a new approach for the estimation of the number of paths that is inherent to the proposed IS-based JADE algorithm. In Section 10, we assess through exhaustive computer simulations the performance of the new estimator and benchmark it against a variety of existing JADE techniques. There, we also assess the localization capabilities of the proposed algorithm using real-world channel measurements. Finally, we draw out some concluding remarks in Section 11.

We define beforehand some of the common notations that will be adopted in this paper. Vectors and matrices are represented in lower- and upper-case bold fonts, respectively. Moreover, $\{.\}^T$ and $\{.\}^H$ denote the conjugate and Hermitian (i.e., transpose conjugate) operators and $\det\{.\}$ returns the determinant of any square matrix. The Euclidean norm of any vector is denoted as $\|.\|$ and $\mathbf{I}_N$ denotes the $(N \times N)$ identity matrix. For any matrix $\mathbf{X}$, $[\mathbf{X}]_q$ and $[\mathbf{X}]_{l,k}$ denote its qth column and (l, k)th entry, respectively. The kronecker product of any two matrices $\mathbf{X}$ and $\mathbf{Y}$ is denoted as $\mathbf{X} \otimes \mathbf{Y}$. In addition, $\{.\}^*$, $\angle\{.\}$, and $|.|$ return the conjugate, angle, and modulus of any complex number, respectively. The complementary cumulative distribution function (CCDF) of a given random variable (RV), X, is denoted as $F_c(x) \triangleq Pr[X \geq x]$. Finally, $\mathbb{E}\{.\}$ stands for statistical expectation, j is the pure complex number that verifies $j^2 = -1$, and the notation $\triangleq$ is used for definitions.

2 OVERVIEW OF RELATED WORKS

Unlike JADE, the separate (or disjoint) estimation of either the time delays or the directions of arrival (DOA) has been heavily investigated for decades now. For prior works on DOA-only and TD-only estimation, see [14], [15] and [16], [17] and references therein, respectively. In comparison with disjoint estimation techniques which first estimate the

delays and then the corresponding angles, the joint estimation of these space-time parameters (i.e., JADE) is more accurate in cases where multiple rays have nearly equal delays or angles [2]. Moreover, contrarily to JADE, the number of estimated angles in DOA-only estimation schemes must be smaller than the number of antennae. Thus DOA-only estimators would require large-size antenna arrays in highly dense multipath environments.

So far, a number of JADE techniques have been reported in the literature, except the unitary matrix pencil (UMP)-based approach proposed recently [12], all the existing solutions are geared toward single-carrier systems. Roughly speaking, they can be broadly categorized into two major categories: subspace-based and ML-based estimators. Most of the subspace-based techniques are built upon the well-known MUSIC and ESPRIT algorithms [18], [19], [20]. In practice, subspace-based approaches are more attractive due to their reduced computational load. However, they are usually suboptimal and suffer from severe performance degradation (both in terms of resolution and estimation accuracy) for low SNR levels and/or closely-spaced paths. ML approaches, however, are known to enjoy higher accuracy and enhanced resolution capabilities. Yet, despite their promising advantages, their computational complexity has been often considered as the major culprit for a widespread reluctance of designers to their implementation in practice.

In the specific JADE context, to the best of our knowledge only two ML estimators have been so far introduced but only for narrowband signals. The very first ML solution was proposed by Wax et al. in [21] which is *iterative* in nature and thus will be referred to, hereafter, as the iterative ML (IML) estimator. The other ML solution introduced later in [22] is also *iterative* and based on the space-alternating generalized expectation maximization (SAGE) algorithm. However, like any *iterative* approach, the performance of these two ML estimators is closely tied to the initial knowledge about the unknown parameters, i.e., they will not converge to the global maximum of the log-likelihood function (LLF) if their initial guesses are not reliable. Besides, for both *iterative* ML estimators, a fixed sampling grid is selected to serve as a possible set of all candidate estimates for the unknown TDs and AoAs. Then, by assuming all true (unknown) parameters to be exactly on the selected grid, IML and SAGE attempt to maximize the LLF iteratively. Consequently, they suffer from the inevitable off-grid problem which arises in practical situations where some of the true TDs and/or AoAs do not lie on the sampling grid. For accurate estimation, it is compulsory to use a densely-sampled grid since it reduces the gap between the true parameters and their nearest points on the grid. However, as "there is no free lunch", the cost of a dense grid sampling is the excessive increase in computational complexity.

These problems, among many others, have spurred a widespread belief that resorting to suboptimal subspace-based solutions is inevitable by trading estimation accuracy for lower complexity. This paper challenges that basic percept by introducing a novel ML JADE technique that beats state-of-the-art subspace-based methods both in terms of accuracy and complexity. Most remarkably, the new ML estimator is statistically efficient since it reaches the CRLB at SNR levels as low as -10 dB.

The proposed estimator builds upon the global maximization theorem of Pincus [23] and the importance sampling (IS) concept [24]. In particular, owing to a very accurate

approximation of the concentrated likelihood function, we transform the original *multi-dimensional* optimization problem into multiple *two-dimensional* optimization ones resulting thereby in tremendous computational savings. Even more, the underlying two-dimensional optimization problems are totally disjoint and, as such, they can be performed separately in practice. From this perspective, the new IS-based ML estimator lends itself to a very attractive parallel computing implementation that can be efficiently executed on nowadays multiprocessor platforms.

The combination of Pincus' theorem and IS concept has been previously applied to many fundamental estimation problems. To the best of our knowledge, however, this elegant combination was first pioneered by Kay and Saha in [25] in the context of multiple frequencies estimation. There, it was shown for the very first time that joint ML estimation of multiple frequencies boils down to the computation of sample mean estimates from a number of realizations generated according to a carefully designed importance function (or pseudo-pdf). Pincus' theorem along with the IS concept were later on applied by Kay et al. to the estimation of chirp signals' parameters [26], sources' DOAs estimation with antenna arrays [15], as well as, joint angle and Doppler estimation in [27]. They were also successfully applied in the context of joint CFO and channel estimation under: i) single-user OFDMA communications [28], and ii) multiuser MIMO-OFDM communications with optimal training sequences design [29]. More recently, these powerful tools were leveraged in the context of TDOA-based source localization [30], non-data-aided (NDA) timing recovery [31], as well as, time delays acquisition in multipath environments [17]. In all these works, the combination of Pincus' theorem with the IS approach resulted in remarkable improvements both from estimation performance and computational complexity viewpoints.

3   SYSTEM MODEL

We will derive our estimator for multi-carrier transmissions and the minor changes that need to be accounted for when dealing with a single-carrier system will be briefly highlighted in Section 6. To start with, consider an antennae array consisting of P antenna elements immersed in a homogeneous medium in the far field of one source that is transmitting a planar wave. The known transmitted signal is modulated over $M + 1$ subcarriers. After undergoing multiple reflections, it impinges on the receiving antenna array from $\bar{Q}$ different angles $(\bar{\alpha}_1, \bar{\alpha}_2, \ldots, \bar{\alpha}_{\bar{Q}})$ with associated time delays $(\bar{\tau}_1, \bar{\tau}_2, \ldots, \bar{\tau}_{\bar{Q}}) \subset [0, \tau_{\max}]^{\bar{Q}}$ where $\tau_{\max}$ can be as large as desired. Note here that we use the overbar symbol to distinguish the true AoAs and TDs, $\bar{\alpha}_q$ and $\bar{\tau}_q$, from the unknown generic variables, α_q and τ_q, that will be used later in the algorithm.[1] We also denote the actual channel frequency response (CFR) over the $\{m^{th}\}_{M=-M/2}^{M/2}$ subcarrier and $\{p^{th}\}_{P=1}^{P}$ antenna element as $\bar{h}_p(m)$ whose expression was derived in [12] as follows (for more details, the reader is referred to [32])

$$\bar{h}_p(m) = \sum_{q=1}^{\bar{Q}} \bar{\xi}_q e^{-j2\pi f_c \bar{\tau}_q} e^{-j2\pi m \Delta f \bar{\tau}_q} e^{-j2\pi \varphi_{p,m}(\bar{\alpha}_q)}. \quad (1)$$

In (1), f_c and Δf stand, respectively, for the carrier frequency and subcarrier spacing while $\{\bar{\xi}_q\}_q^Q$ stand for the actual path gain coefficients which are assumed to be unknown as well. Moreover, the functions $\varphi_{p,m}(\alpha)$ represent some real-valued angular transformations that depend on the array geometry. Typically, uniform linear arrays (ULAs) and uniform circular arrays (UCAs) remain by far the most studied cases in the open literature. For these two popular configurations, the underlying angular transformations are given by

$$\varphi_{p,m}(\alpha) = \begin{cases} \dfrac{d(f_c + m\Delta f)}{c}(p-1)\sin(\alpha), & \text{(ULA)} \\[2ex] \dfrac{d(f_c + m\Delta f)}{c} \dfrac{\cos(\alpha - 2[p-1]\pi/P)}{2\sin(\pi/P)}, & \text{(UCA)}, \end{cases}$$

where $d = \lambda/2$ is the separation between consecutive antenna elements, and c is the speed of light.

Given the transmitted signal and the received data, an estimate, $h_p(m)$, for the actual CFR $\bar{h}_p(m)$ in (1) can be readily obtained by applying any data-aided (DA) channel estimation technique, e.g., the least-squares method. By doing so, one has access to the following implicit observation model:

$$h_p(m) = \sum_{q=1}^{\bar{Q}} \bar{\gamma}_q e^{-j2\pi m \Delta f \bar{\tau}_q} e^{-j2\pi \varphi_p(\bar{\alpha}_q)} + w_p(m), \quad (2)$$

in which we defined $\bar{\gamma}_q \triangleq \bar{\xi}_q e^{-j2\pi f_c \bar{\tau}_q}$ for $q = 1, \ldots, \bar{Q}$ that are some unknown but constant coefficients across all the subcarriers and antenna elements. Moreover, $w_p(m)$ are the residual estimation noise components which are assumed to be spatially white and uncorrelated between subcarriers. Statistically, they are modeled by zero-mean complex Gaussian random processes with independent real and imaginary parts each of variance $\sigma^2/2$.

For mathematical convenience, we now group all the unknown multipath parameters in the following three vectors: $\bar{\boldsymbol{\alpha}} = [\bar{\alpha}_1, \bar{\alpha}_2, \ldots, \bar{\alpha}_{\bar{Q}}]^T$, $\bar{\boldsymbol{\tau}} = [\bar{\tau}_1, \bar{\tau}_2, \ldots, \bar{\tau}_{\bar{Q}}]^T$, and $\bar{\boldsymbol{\gamma}} = [\bar{\gamma}_1, \bar{\gamma}_2, \ldots, \bar{\gamma}_{\bar{Q}}]^T$. We further gather the channel estimates in (43) across all the antenna elements at each mth subcarrier into a single vector, $\mathbf{h}(m) = [h_1(m), h_2(m), \ldots, h_P(m)]^T$, given by

$$\mathbf{h}(m) = \sum_{q=1}^{\bar{Q}} \mathbf{a}_m(\bar{\alpha}_q) \bar{\gamma}_q \, e^{-j2\pi m \Delta f \bar{\tau}_q} + \mathbf{w}(m), \quad (3)$$

where $\mathbf{w}(m) = [w_1(m), w_2(m), \ldots, w_P(m)]^T$ is the corresponding noise vector and

$$\mathbf{a}_m(\alpha) \triangleq \left[e^{-j2\pi \varphi_{1,m}(\alpha)}, \, e^{-j2\pi \varphi_{2,m}(\alpha)}, \ldots, \, e^{-j2\pi \varphi_{P,m}(\alpha)} \right]^T, \quad (4)$$

is the array *steering vector* defined for any direction α. Our goal in the remainder of this paper is to jointly estimate the parameters $\{\bar{\alpha}_q\}_q^Q$ and $\{\bar{\tau}_q\}_q^Q$ along with $\bar{Q}$ given the $M + 1$ vectors $\{\mathbf{h}(m)\}_{m=-M/2}^{M/2}$.

4   DERIVATION OF THE CONCENTRATED LIKELIHOOD FUNCTION

In this section, we will derive the *concentrated* likelihood function that depends on the parameters of interest only [33], namely $\bar{\boldsymbol{\tau}}, \bar{\boldsymbol{\alpha}}$. In fact, since $\mathbf{w}(m) \backsim \mathcal{N}(\mathbf{0}, \sigma^2 \mathbf{I}_P)$, it can be

---

1. For the same reasons, we use $\bar{Q}$ to denote the true unknown number of paths that will be estimated later in Section 7.

shown that the actual LLF (after dropping the constant terms) is given by[2]

$$\mathcal{L}(\boldsymbol{\alpha}, \boldsymbol{\tau}, \boldsymbol{\gamma}) = \sum_{m=-\frac{M}{2}}^{\frac{M}{2}} \left\| \mathbf{h}(m) - \sum_{q=1}^{\bar{Q}} \mathbf{a}_m(\alpha_q) \gamma_q e^{-j2\pi m \Delta f \bar{\tau}_q} \right\|^2, \quad (5)$$

where $\boldsymbol{\tau}$, $\boldsymbol{\alpha}$, and $\boldsymbol{\gamma}$ stand for any candidate values for $\bar{\boldsymbol{\tau}}$, $\bar{\boldsymbol{\alpha}}$, and $\bar{\boldsymbol{\gamma}}$, respectively. Now, define the $(M\bar{Q} \times \bar{Q})$ matrix

$$\boldsymbol{\Phi}(\boldsymbol{\tau}) \triangleq \left[\boldsymbol{\Phi}_{-M/2}(\boldsymbol{\tau})^T \, \boldsymbol{\Phi}_{-M/2+1}(\boldsymbol{\tau})^T \ldots \, \boldsymbol{\Phi}_{M/2}(\boldsymbol{\tau})^T \right]^T, \quad (6)$$

with $\{\boldsymbol{\Phi}_m(\boldsymbol{\tau})\}_{m=-M/2}^{M/2}$ being the following $(\bar{Q} \times \bar{Q})$ diagonal matrix

$$\boldsymbol{\Phi}_m(\boldsymbol{\tau}) \triangleq \mathrm{diag}\left(e^{-j\omega_m \tau_1}, e^{-j\omega_m \tau_2}, \ldots, e^{-j\omega_m \tau_{\bar{Q}}}\right), \quad (7)$$

and $\omega_m = 2\pi m \Delta f$. Therefore, by letting $\mathbf{A}_m(\boldsymbol{\alpha}) \triangleq [\mathbf{a}_m(\alpha_1) \, a_m(\alpha_2) \, \ldots \, \mathbf{a}_m(\alpha_{\bar{Q}})]$ and defining the following array *steering matrix*:

$$\mathbf{A}(\boldsymbol{\alpha}) = \left\{ \begin{array}{cccc} \mathbf{A}_{-M/2}(\boldsymbol{\alpha}) & 0 & \ldots & 0 \\ 0 & \mathbf{A}_{-M/2+1}(\boldsymbol{\alpha}) & & \vdots \\ \vdots & & \ddots & 0 \\ 0 & \ldots & 0 & \mathbf{A}_{M/2}(\boldsymbol{\alpha}) \end{array} \right\}, \quad (8)$$

it can be shown that (5) is equivalent to

$$\mathcal{L}(\boldsymbol{\alpha}, \boldsymbol{\tau}, \boldsymbol{\gamma}) = \left\| \mathbf{h} - \mathbf{A}(\boldsymbol{\alpha})\boldsymbol{\Phi}(\boldsymbol{\tau})\boldsymbol{\gamma} \right\|^2, \quad (9)$$

where $\mathbf{h} \triangleq \left[\mathbf{h}(\omega_{-M/2})^T \mathbf{h}(\omega_{-M/2+1})^T \ldots \mathbf{h}(\omega_{M/2})^T \right]^T$. Maximizing (9) jointly with respect to $\boldsymbol{\tau}$, $\boldsymbol{\alpha}$, and $\boldsymbol{\gamma}$ is extremely challenging. Yet, significant computational savings follow from the observation that for any given $\boldsymbol{\tau}$ and $\boldsymbol{\alpha}$, the problem of finding the optimal $\boldsymbol{\gamma}$ becomes a linear least squares (LS) problem [34] whose solution is given by

$$\widehat{\boldsymbol{\gamma}}_{\mathrm{MLE}} = \left[\underbrace{\mathbf{A}(\boldsymbol{\alpha})\boldsymbol{\Phi}(\boldsymbol{\tau})}_{\triangleq \mathbf{D}} \right]^\dagger \mathbf{h}, \quad (10)$$

where $\mathbf{D}^\dagger$ is the Moore-Penrose pseudo-inverse of $\mathbf{D}$ given by $\mathbf{D}^\dagger = \left(\mathbf{D}^H \mathbf{D}\right)^{-1} \mathbf{D}^H$. Note here that $\mathbf{D}$ has full column rank and, therefore, $\left(\mathbf{D}^H \mathbf{D}\right)^{-1}$ always exists. Now, by substituting $\widehat{\boldsymbol{\gamma}}_{\mathrm{MLE}}$ for $\boldsymbol{\gamma}$ back in (9) and resorting to some straightforward algebraic manipulations, we obtain the so-called *concentrated* likelihood function which depends solely on $\boldsymbol{\alpha}$ and $\boldsymbol{\tau}$

$$\mathcal{L}_c(\boldsymbol{\alpha}, \boldsymbol{\tau}) = \mathbf{h}^H \mathbf{D}(\mathbf{D}^H \mathbf{D})^{-1} \mathbf{D}^H \mathbf{h}. \quad (11)$$

The joint ML estimates of $\bar{\boldsymbol{\alpha}}$ and $\bar{\boldsymbol{\tau}}$ are then obtained as the solution to the following reduced-dimension optimization problem

$$[\widehat{\boldsymbol{\alpha}}_{\mathrm{MLE}}, \, \widehat{\boldsymbol{\tau}}_{\mathrm{MLE}}] = \underset{\boldsymbol{\alpha}, \boldsymbol{\tau}}{\mathrm{argmax}} \, \mathcal{L}_c(\boldsymbol{\alpha}, \boldsymbol{\tau}). \quad (12)$$

Once $\widehat{\boldsymbol{\alpha}}_{\mathrm{MLE}}$ and $\widehat{\boldsymbol{\tau}}_{\mathrm{MLE}}$ are obtained, they can be substituted back in (10) in order to find the MLEs for all the unknown path gains, i.e., $\widehat{\boldsymbol{\gamma}}_{\mathrm{MLE}}$.

---

2. Note here that, for ease of notation, we do not show explicitly the dependence of the LLF on $\{\mathbf{h}(m)\}_{m=-M/2}^{M/2}$ in the left-hand side of (5).

5 GLOBAL MAXIMIZATION OF THE CLF

5.1 Pincus' Theorem and the IS Concept

As done previously within the framework of other estimation problems (see [15], [25], [26], [27], [28], [29], [30], [31], and references therein), we will resort to Pincus' theorem [23] and the powerful IS concept [38] in order to solve the multidimensional optimization problem in (12). The theorem proposed by Pincus in [23] simply states that the global maximum of any continuous $\bar{Q}$-dimensional function, $f(\boldsymbol{\theta})$, is reached at the vector $\widehat{\boldsymbol{\theta}} = [\widehat{\theta}_1, \widehat{\theta}_2, \ldots, \widehat{\theta}_{\bar{Q}}]$ whose $\{q^{th}\}_{q=1}^{\bar{Q}}$ entry is given by

$$\widehat{\theta}_q = \lim_{\rho \to +\infty} \frac{\int \cdots \int \theta_q e^{\rho f(\boldsymbol{\theta})} d\boldsymbol{\theta}}{\int \cdots \int e^{\rho f(\boldsymbol{\theta})} d\boldsymbol{\theta}}. \quad (13)$$

The limit involved in (13) is approximated for some sufficiently high value ρ_0 of ρ as follows:

$$\widehat{\theta}_q = \frac{\int \cdots \int \alpha_q e^{\rho_0 f(\boldsymbol{\theta})} d\boldsymbol{\theta}}{\int \cdots \int e^{\rho_0 f(\boldsymbol{\theta})} d\boldsymbol{\theta}}. \quad (14)$$

Applying this general result to our estimation problem with $\boldsymbol{\theta} \triangleq [\boldsymbol{\alpha}, \boldsymbol{\tau}]^T$ and $f(\boldsymbol{\theta}) \triangleq \mathcal{L}_c(\boldsymbol{\alpha}, \boldsymbol{\tau})$ leads to the following expressions for the required MLEs (each in terms of $2\bar{Q}$-dimensional integrals) for $q = 1, 2, \ldots, \bar{Q}$

$$\widehat{\bar{\tau}}_{q, \mathrm{MLE}} = \int \cdots \int \tau_q \, \bar{\mathcal{L}}_c(\boldsymbol{\alpha}, \boldsymbol{\tau}) d\boldsymbol{\alpha} d\boldsymbol{\tau}, \quad (15)$$

$$\widehat{\bar{\alpha}}_{q, \mathrm{MLE}} = \int \cdots \int \alpha_q \, \bar{\mathcal{L}}_c(\boldsymbol{\alpha}, \boldsymbol{\tau}) d\boldsymbol{\alpha} d\boldsymbol{\tau}, \quad (16)$$

where $\bar{\mathcal{L}}_c(\boldsymbol{\alpha}, \boldsymbol{\tau})$ is the *normalized* CLF defined as

$$\bar{\mathcal{L}}_c(\boldsymbol{\alpha}, \boldsymbol{\tau}) \triangleq \frac{e^{\rho_0 \mathcal{L}_c(\boldsymbol{\alpha}, \boldsymbol{\tau})}}{\int \cdots \int e^{\rho_0 \mathcal{L}_c(\boldsymbol{\alpha}, \boldsymbol{\tau})} d\boldsymbol{\alpha} d\boldsymbol{\tau}}. \quad (17)$$

Intuitively, as ρ_0 tends to infinity, $\bar{\mathcal{L}}_c(\boldsymbol{\alpha}, \boldsymbol{\tau})$ becomes a Dirac-delta function centered at the true maximum of $\mathcal{L}_c(\boldsymbol{\alpha}, \boldsymbol{\tau})$ whose location is indeed given by the set of integrals in (15) and (16). In our attempt to avoid multi-dimensional grid search, it may appear here at first sight that we have we ended up dealing with a multi-dimensional integration bearing the very same practical difficulties. By closely inspecting (17), however, it turns out that the *normalized* CLF, $\bar{\mathcal{L}}_c(\boldsymbol{\alpha}, \boldsymbol{\tau})$, has all the properties of a pdf since it is non-negative and integrates to one. Consequently, we will term it in the sequel as "*pseudo-pdf*" since strictly speaking the involved working variables $\boldsymbol{\alpha}$ and $\boldsymbol{\tau}$ are not truly random. Yet, by hypothetically assuming them to be random vectors that are jointly distributed according to $\bar{\mathcal{L}}_c(\boldsymbol{\alpha}, \boldsymbol{\tau})$, the MLEs in (15) and (16) can be alternatively regarded as statistical expectations, i.e., for $q = 1, 2, \ldots, \bar{Q}$, we have

$$\widehat{\bar{\tau}}_{q, \mathrm{MLE}} = \mathbb{E}_{\boldsymbol{\alpha}, \boldsymbol{\tau}}\{\tau_q\} \quad \text{and} \quad \widehat{\bar{\alpha}}_{q, \mathrm{MLE}} = \mathbb{E}_{\boldsymbol{\alpha}, \boldsymbol{\tau}}\{\alpha_q\}. \quad (18)$$

Thus, if one is able to generate R realizations, $\{\boldsymbol{\tau}^{(r)}\}_{r=1}^R$ and $\{\boldsymbol{\alpha}^{(r)}\}_{r=1}^R$, using the joint *pseudo-pdf* $\bar{\mathcal{L}}_c(\boldsymbol{\tau}, \boldsymbol{\alpha})$, then it will be

very accurate to approximate the expectations in (18) by their sample mean estimates as follows:

$$\widehat{\overline{\tau}}_{q,\,\mathrm{MLE}} = \frac{1}{R}\sum_{r=1}^{R} \tau_q^{(r)} \quad \text{and} \quad \widehat{\overline{\alpha}}_{q,\,\mathrm{MLE}} = \frac{1}{R}\sum_{r=1}^{R} \alpha_q^{(r)}. \quad (19)$$

Clearly, as the number of realizations R used in (19) increases, the variances of the two sample mean estimates above decrease making them approach the global maximum of the CLF [38]. Unfortunately, the pseudo-pdf $\bar{\mathcal{L}}_c(\boldsymbol{\alpha}, \boldsymbol{\tau})$ is extremely non-linear and as such cannot be practically used to generate $\{\boldsymbol{\tau}^{(r)}\}_{r=1}^{R}$ and $\{\boldsymbol{\alpha}^{(r)}\}_{r=1}^{R}$. To sidestep this problem, one can resort to the importance sampling concept [15], [25] and rewrite (15) and (16) in the following equivalent forms:

$$\widehat{\overline{\tau}}_{q,\mathrm{MLE}} = \int \cdots \int \tau_q \frac{\bar{\mathcal{L}}_c(\boldsymbol{\alpha}, \boldsymbol{\tau})}{\bar{\mathcal{G}}(\boldsymbol{\alpha}, \boldsymbol{\tau})} \bar{\mathcal{G}}(\boldsymbol{\alpha}, \boldsymbol{\tau}) d\boldsymbol{\alpha} d\boldsymbol{\tau}, \quad (20)$$

$$\widehat{\overline{\alpha}}_{q,\mathrm{MLE}} = \int \cdots \int \alpha_q \frac{\bar{\mathcal{L}}_c(\boldsymbol{\alpha}, \boldsymbol{\tau})}{\bar{\mathcal{G}}(\boldsymbol{\alpha}, \boldsymbol{\tau})} \bar{\mathcal{G}}(\boldsymbol{\alpha}, \boldsymbol{\tau}) d\boldsymbol{\alpha} d\boldsymbol{\tau}, \quad (21)$$

for some $\bar{\mathcal{G}}(\boldsymbol{\alpha}, \boldsymbol{\tau})$ which is another pseudo-pdf—called *importance function*—to be designed as close as possible to $\bar{\mathcal{L}}_c(\boldsymbol{\alpha}, \boldsymbol{\tau})$ while allowing at the same time the easy generation of the required vector realizations $\{\boldsymbol{\tau}^{(r)}\}_{r=1}^{R}$ and $\{\boldsymbol{\alpha}^{(r)}\}_{r=1}^{R}$. By doing so, the MLEs in (20) and (21) are interpreted as expected values of transformed RVs, i.e.,

$$\widehat{\overline{\tau}}_{q,\,\mathrm{MLE}} = \mathbb{E}_{\boldsymbol{\alpha}, \boldsymbol{\tau}} \big\{ \eta(\boldsymbol{\tau}, \boldsymbol{\alpha}) \tau_q \big\} \quad (22)$$

$$\widehat{\overline{\alpha}}_{q,\,\mathrm{MLE}} = \mathbb{E}_{\boldsymbol{\alpha}, \boldsymbol{\tau}} \big\{ \eta(\boldsymbol{\alpha}, \boldsymbol{\tau}) \alpha_q \big\}, \quad (23)$$

where $\eta(\boldsymbol{\alpha}, \boldsymbol{\tau})$ is defined as the following ratio:

$$\eta(\boldsymbol{\alpha}, \boldsymbol{\tau}) \triangleq \frac{\bar{\mathcal{L}}_c(\boldsymbol{\alpha}, \boldsymbol{\tau})}{\bar{\mathcal{G}}(\boldsymbol{\alpha}, \boldsymbol{\tau})}. \quad (24)$$

If $\bar{\mathcal{G}}(\boldsymbol{\alpha}, \boldsymbol{\tau})$ is carefully designed, the expectations in (22) and (23) can be computed at any desired degree of accuracy (by increasing R) using the corresponding sample mean estimates. The appropriate choice of the importance function, $\bar{\mathcal{G}}(\boldsymbol{\alpha}, \boldsymbol{\tau})$, will be discussed in the following section. But before delving into details, we mention beforehand that it must be separable in terms of the $\bar{Q}$ angle-delay pairs $\{(\alpha_q, \tau_q)\}_{q=1}^{\bar{Q}}$ in order to facilitate the process of generating the required R vector realizations. In other words, our ultimate goal is to design $\bar{\mathcal{G}}(\boldsymbol{\alpha}, \boldsymbol{\tau})$ in a way that allows it to be factorized as follows:

$$\bar{\mathcal{G}}(\boldsymbol{\alpha}, \boldsymbol{\tau}) = \prod_{q=1}^{\bar{Q}} \bar{g}_q(\alpha_q, \tau_q). \quad (25)$$

This will allow us to interpret $\bar{\mathcal{G}}(\boldsymbol{\alpha}, \boldsymbol{\tau})$ as a multivariate pseudo-pdf that corresponds to a set of *independent* bivariate random variables. Hence, instead of generating realizations for $\bar{Q}$-dimensional random vectors $\boldsymbol{\alpha}$ and $\boldsymbol{\tau}$ directly using $\bar{\mathcal{G}}(\boldsymbol{\alpha}, \boldsymbol{\tau})$, one can easily generate independent realizations for *bivariate* random variables $\{(\alpha_q, \tau_q)\}_{q=1}^{\bar{Q}}$ using $\{\bar{g}_q(\alpha_q, \tau_q)\}_{q}^{\bar{Q}}$. In order to reduce the variance of estimation errors, however, it is preferable to design $\bar{\mathcal{G}}(\boldsymbol{\alpha}, \boldsymbol{\tau})$ upon an appropriate approximation of $\bar{\mathcal{L}}_c(\boldsymbol{\alpha}, \boldsymbol{\tau})$.

5.2 Approximation of the CLF and Appropriate Choice for $\bar{\mathcal{G}}(\boldsymbol{\alpha}, \boldsymbol{\tau})$

First, by revisiting (46), one can easily recognize that the original CLF, $\mathcal{L}_c(\boldsymbol{\alpha}, \boldsymbol{\tau})$, cannot be directly expressed as a separable function due to the presence of the matrix inverse $(\mathbf{D}^H \mathbf{D})^{-1}$. Fortunately, though, we show in the sequel that $\mathbf{D}^H \mathbf{D}$ can be accurately approximated by a diagonal matrix. In fact, by recalling the expression of $\mathbf{D}$ in (10), we notice that the delay coming from the antenna array is negligible when compared with τ_l (i.e., $p\, d \sin(\alpha_l)/c\tau_l$), it follows that:

$$\mathbf{D} = \big[\mathbf{I}_M \otimes \mathbf{A}_0(\boldsymbol{\alpha}) \big] \boldsymbol{\Phi}(\boldsymbol{\tau}). \quad (26)$$

By using some basic properties of the Kronecker product, the matrix $\mathbf{D}^H \mathbf{D}$ can be written as

$$\begin{aligned} \mathbf{D}^H \mathbf{D} &= \boldsymbol{\Phi}(\boldsymbol{\tau})^H \big[\mathbf{I}_{M+1} \otimes \mathbf{A}(\boldsymbol{\alpha})^H \big] \big[\mathbf{I}_{M+1} \otimes \mathbf{A}(\boldsymbol{\alpha}) \big] \boldsymbol{\Phi}(\boldsymbol{\tau}), \\ &= \boldsymbol{\Phi}(\boldsymbol{\tau})^H \Big(\mathbf{I}_{M+1} \otimes \big[\mathbf{A}(\boldsymbol{\alpha})^H \mathbf{A}(\boldsymbol{\alpha}) \big] \Big) \boldsymbol{\Phi}(\boldsymbol{\tau}), \end{aligned} \quad (27)$$

Then, by noticing that $\mathbf{I}_{M+1} \otimes \big[\mathbf{A}_0(\boldsymbol{\alpha})^H \mathbf{A}_0(\boldsymbol{\alpha}) \big]$ is a block-diagonal matrix, it can be shown that

$$\mathbf{D}^H \mathbf{D} = \sum_{m=-M/2}^{M/2} \boldsymbol{\Phi}_m(\boldsymbol{\tau})^H \mathbf{A}_0(\boldsymbol{\alpha})^H \mathbf{A}_0(\boldsymbol{\alpha}) \boldsymbol{\Phi}_m(\boldsymbol{\tau}). \quad (28)$$

Next, by recalling that the lth column of the steering matrix is $\big[\mathbf{A}_0(\boldsymbol{\alpha}) \big]_l = \mathbf{a}_0(\alpha_l)$ and since $\boldsymbol{\Phi}_m(\boldsymbol{\tau})$ is a diagonal matrix, we immediately have

$$\begin{aligned} [\mathbf{A}_0(\boldsymbol{\alpha}) \boldsymbol{\Phi}_m(\boldsymbol{\tau})]_l &= [\boldsymbol{\Phi}_m(\boldsymbol{\tau})]_{l,l} [\mathbf{A}_0(\boldsymbol{\alpha})]_l \\ &= e^{-j\omega_m \tau_l} \mathbf{a}_0(\alpha_l). \end{aligned}$$

The (l, k)th entry of $\mathbf{D}^H \mathbf{D}$ is thus obtained as

$$\begin{aligned} [\mathbf{D}^H \mathbf{D}]_{l,k} &= \sum_{m=-M/2}^{M/2} \big([\mathbf{A}_0(\boldsymbol{\alpha}) \boldsymbol{\Phi}_m(\boldsymbol{\tau})]_l \big)^H [\mathbf{A}_0(\boldsymbol{\alpha}) \boldsymbol{\Phi}_m(\boldsymbol{\tau})]_k, \\ &= \sum_{m=-M/2}^{M/2} e^{j\omega_m(\tau_l - \tau_k)} \mathbf{a}_0(\alpha_l)^H \mathbf{a}_0(\alpha_k), \\ &= \sum_{m=-M/2}^{M/2} e^{j\omega_m(\tau_l - \tau_k)} \\ &\quad \times \sum_{p=1}^{P} e^{-j2\pi[\varphi_p(\alpha_k) - \varphi_p(\alpha_l)]}. \end{aligned} \quad (29)$$

In particular, all the diagonal elements are expressed as

$$[\mathbf{D}^H \mathbf{D}]_{k,k} = P(M+1). \quad (30)$$

Due to the destructive superposition (for $l \neq k$) of the complex exponentials[3] in (29), one could expect the off-diagonal entries of $\mathbf{D}^H \mathbf{D}$ to be very small compared to the diagonal ones thereby allowing the following much useful approximation

$$\mathbf{D}^H \mathbf{D} \approx P(M+1) \mathbf{I}_{\bar{Q}}. \quad (31)$$

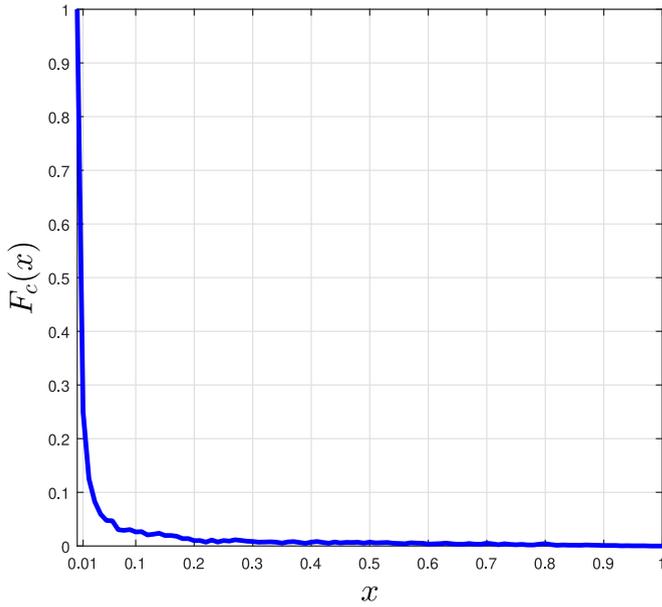3. This is reminiscent of multipath fading in wireless channels.

Fig. 1. CCDF of the magnitude of the ratio between the off-diagonal and diagonal entries of the matrix $\mathbf{D}^H\mathbf{D}$, using $M+1 = 245$ subcarriers and a ULA configuration of $P = 6$ receiving antenna elements.

To see this, we define

$$\beta_{l,k} \triangleq \frac{\left(\sum_{m=-M/2}^{M/2} e^{j\omega_m(\tau_l - \tau_k)}\right)\left(\sum_{p=1}^{P} e^{-j2\pi[\varphi_p(\alpha_k) - \varphi_p(\alpha_l)]}\right)}{P(M+1)}, \quad (32)$$

as the ratio of the off-diagonal over diagonal entries of $\mathbf{D}^H\mathbf{D}$. Then, we generate a large number of couples $(\tau_l, \tau_k) \curvearrowright U[0, \tau_{\max}]^2$ and $(\alpha_l, \alpha_k) \curvearrowright U[-\pi/2, \pi/2]^2$ and inject them into (32) in order to compute the CCDF, $F_c(x) = Pr[|\beta_{l,k}| \geq x]$, depicted in Fig. 1. There, it can be seen that the off-diagonal elements of $\mathbf{D}^H\mathbf{D}$ can indeed be neglected in front of its diagonal ones since $|\beta_{l,k}|$ has an almost-zero probability to exceed 0.1 for all $l \neq k$. Therefore, (31) is a valid and accurate approximation for $\mathbf{D}^H\mathbf{D}$ which is used in (46) to obtain the following accurate approximation

$$\mathcal{L}_c(\boldsymbol{\alpha}, \boldsymbol{\tau}) \approx \frac{1}{P(M+1)}\mathbf{h}^H\mathbf{D}\mathbf{D}^H\mathbf{h}. \quad (33)$$

Recalling from (10) that $\mathbf{D} = \mathbf{A}(\boldsymbol{\alpha})\boldsymbol{\Phi}(\boldsymbol{\tau})$, it follows that:

$$\mathcal{L}_c(\boldsymbol{\alpha}, \boldsymbol{\tau}) \approx \frac{1}{P(M+1)}\left\|\boldsymbol{\Phi}(\boldsymbol{\tau})^H\mathbf{A}(\boldsymbol{\alpha})^H\mathbf{h}\right\|^2. \quad (34)$$

Now, by recalling that

$$\mathbf{h} = \left[\mathbf{h}(-M/2)^T \ \mathbf{h}(-M/2+1)^T \ \ldots \ \mathbf{h}(M/2)^T\right]^T, \quad (35)$$

and using (6) it can be shown that

$$\boldsymbol{\Phi}(\boldsymbol{\tau})^H\mathbf{A}(\boldsymbol{\alpha})^H\mathbf{h} = \sum_{m=-M/2}^{M/2}\left[\mathbf{A}_m(\boldsymbol{\alpha})\boldsymbol{\Phi}_m(\boldsymbol{\tau})\right]^H\mathbf{h}(m). \quad (36)$$

Therefore, it follows from (34) that

$$\mathcal{L}_c(\boldsymbol{\alpha}, \boldsymbol{\tau}) \approx \frac{1}{P(M+1)}\sum_{q=1}^{\bar{Q}}\left|\sum_{m=-M/2}^{M/2}\left[\mathbf{A}_m(\boldsymbol{\alpha})\boldsymbol{\Phi}_m(\boldsymbol{\tau})\right]_q^H\mathbf{h}(m)\right|^2. \quad (37)$$

Starting form (37) and resorting to some straightforward algebraic manipulations, we obtain the following much useful approximation for the CLF

$$\mathcal{L}_c(\boldsymbol{\alpha}, \boldsymbol{\tau}) \approx \frac{1}{P(M+1)}\sum_{q=1}^{\bar{Q}}I(\alpha_q, \tau_q), \quad (38)$$

where $I(\alpha, \tau)$ is the periodogram of the signal given by

$$I(\alpha, \tau) = \left|\sum_{p=1}^{P}\sum_{m=-M/2}^{M/2}e^{-j2\pi\varphi_{p,m}(\alpha)}h_p^*(m)e^{-j2\pi\tau\omega_m}\right|^2, \quad (39)$$

in which $h_p(m)$ is the pth element of the vector $\mathbf{h}(m)$. Owing to the decomposition of the *approximate* CLF in (38) as the superposition of the separate contributions pertaining to the $\bar{Q}$ angle-delay pairs, we exploit it below as the *importance function* (upon normalization)

$$\bar{\mathcal{G}}(\boldsymbol{\alpha}, \boldsymbol{\tau}) = \frac{\exp\left\{\rho_1\sum_{q=1}^{\bar{Q}}I(\alpha_q, \tau_q)\right\}}{\int\cdots\int\exp\left\{\rho_1\sum_{q=1}^{\bar{Q}}I(\alpha_q', \tau_q')\right\}d\boldsymbol{\alpha}'d\boldsymbol{\tau}'}. \quad (40)$$

Note here that the factor $\frac{1}{P(M+1)}$ involved in (38) is absorbed in the new design parameter, $\rho_1 \neq \rho_0$, whose appropriate choice will be discussed later in Section 10. Note as well that $\bar{\mathcal{G}}(\boldsymbol{\alpha}, \boldsymbol{\tau})$ is *separable* in terms of the angle-delay pairs as originally required. Indeed, it can be easily shown that $\bar{\mathcal{G}}(\boldsymbol{\alpha}, \boldsymbol{\tau})$ factorizes as follows:

$$\bar{\mathcal{G}}(\boldsymbol{\alpha}, \boldsymbol{\tau}) = \prod_{q=1}^{\bar{Q}}\bar{g}_{\bar{\alpha}, \bar{\tau}}(\alpha_q, \tau_q), \quad (41)$$

where

$$\bar{g}_{\bar{\alpha}, \bar{\tau}}(\alpha, \tau) = \frac{e^{\rho_1 I(\alpha, \tau)}}{\int\int e^{\rho_1 I(\alpha', \tau')}d\alpha'd\tau'}, \quad (42)$$

is a common bivariate distribution for all angle/delay pairs. Therefore, in order to generate vector realizations $\boldsymbol{\alpha}^{(r)}$ and $\boldsymbol{\tau}^{(r)}$ using the multidimensional distribution $\bar{\mathcal{G}}(\boldsymbol{\alpha}, \boldsymbol{\tau})$, one can easily generate $\bar{Q}$ independent couples $(\alpha_q^{(r)}, \tau_q^{(r)})$ using $\bar{g}_{\bar{\alpha}, \bar{\tau}}(\alpha, \tau)$ then construct $\boldsymbol{\alpha}^{(r)} = [\alpha_1^{(r)}, \alpha_2^{(r)}, \ldots, \alpha_{\bar{Q}}^{(r)}]$ and $\boldsymbol{\tau}^{(r)} = [\tau_1^{(r)}, \tau_2^{(r)}, \ldots, \tau_{\bar{Q}}^{(r)}]$. The process of generating $\{(\alpha_q^{(r)}, \tau_q^{(r)})\}_{q=1}^{\bar{Q}}$ using $\bar{g}_{\bar{\alpha}, \bar{\tau}}(\alpha, \tau)$ is explained in some depth later in Section 7.

6 SPECIAL CASE OF SINGLE-CARRIER SYSTEMS

Assume that a known modulated signal $s(t)$ is transmitted by the source. After sampling the continuous-time received signal at time instants $\{t_m = mT_s\}_{m=0}^{(M-1)}$ where T_s is the sampling period, one obtains the following M samples over each pth antenna

$$x_p(t_m) = \sum_{q=1}^{\bar{Q}}\bar{\xi}_q s(t_m - \bar{\tau}_q)e^{j\pi\varphi_p(\bar{\alpha}_q)} + w_p(t_m), \quad (43)$$

for $m = 0, 2, \ldots, M - 1$. By collecting the samples across all the antenna elements at each mth time index, $\mathbf{x}(t_m) = [x_1(t_m), x_2(t_m), \ldots, x_P(t_m)]^T$, one obatins

$$\mathbf{x}(t_m) = \sum_{q=1}^{\bar{Q}} \mathbf{a}_0(\bar{\alpha}_q)\bar{\xi}_q s(t_m - \bar{\tau}_q) + \mathbf{w}(t_m), \qquad (44)$$

in which $\mathbf{a}_0(\bar{\alpha}_q)$ is obtained from (4) by setting $m = 0$. Then, by using Parseval's identity, it can be shown that the actual LLF is expressed as follows in the case of single-carrier systems

$$\mathcal{L}_{\text{SC}}(\boldsymbol{\alpha}, \boldsymbol{\tau}, \boldsymbol{\gamma}) \approx \sum_{m=0}^{M-1} \left\| \mathbf{x}(\omega_m) - \sum_{q=1}^{\bar{Q}} \mathbf{a}_0(\alpha_q)\gamma_q e^{-j\omega_m \tau_q} s(\omega_m) \right\|^2, \qquad (45)$$

where $\{\mathbf{x}(\omega_m)\}_m$ and $\{s(\omega_m)\}_m$ are, respectively, the DFTs of $\{\mathbf{x}(t_m)\}_m$ and $\{s(t_m)\}_m$ and $\left\{\omega_m = \frac{m}{MT_s}\right\}_{m=0}^{M-1}$ is the mth frequency bin. By following the same derivations as done in the OFDM model in the previous sections, it can be shown that the CLF of SC systems is expressed as follows:

$$\mathcal{L}_c^{\text{SC}}(\boldsymbol{\alpha}, \boldsymbol{\tau}) = \mathbf{x}^H \mathbf{D}(\mathbf{D}^H\mathbf{D})^{-1}\mathbf{D}^H\mathbf{x}, \qquad (46)$$

where $\mathbf{x} \triangleq \left[\mathbf{x}(\omega_1)^T \mathbf{x}(\omega_2)^T \ldots \mathbf{x}(\omega_M)^T\right]^T$ and the matrix D is given by

$$\mathbf{D} = \left[\mathbf{I}_M \otimes \mathbf{A}_0(\boldsymbol{\alpha})\right]\boldsymbol{\Phi}(\boldsymbol{\tau}). \qquad (47)$$

Then, it is easy to show that $\mathbf{D}^H\mathbf{D}$ can also be approximated by a diagonal matrix thereby leading to the same expression for the importance function already obtained in and (41) and (42). The only difference being in the expression of the periodogram which is now given by

$$I_{\text{sc}}(\boldsymbol{\alpha}, \boldsymbol{\tau}) = \left| \sum_{p=1}^{P} e^{j\pi\varphi_p(\alpha)} \sum_{m=0}^{M-1} s(\omega_m)x_p^*(\omega_m)e^{-j2\pi\tau\omega_m} \right|^2, \qquad (48)$$

in which $x_p(\omega_m)$ is the pth element of the vector $\mathbf{x}(\omega_m)$. The remaining derivations hold exactly the same for both single- and multi-carrier systems.

7 GENERATION OF THE REQUIRED REALIZATIONS

A well-known general result from probability theory is that the joint distribution, $\bar{g}_{\bar{\alpha},\bar{\tau}}(\alpha, \tau)$, can be factorized as the product of marginal and conditional pdfs, in two equivalent forms, as follows:

$$\bar{g}_{\bar{\alpha},\bar{\tau}}(\alpha, \tau) = \bar{g}_{\bar{\tau}}(\tau)\bar{g}_{\bar{\alpha}|\bar{\tau}}(\alpha|\tau), \qquad (49)$$

$$\bar{g}_{\bar{\alpha},\bar{\tau}}(\alpha, \tau) = \bar{g}_{\bar{\alpha}}(\alpha)\bar{g}_{\bar{\tau}|\bar{\alpha}}(\tau|\alpha), \qquad (50)$$

where $\bar{g}_{\bar{\tau}}$ [resp., $\bar{g}_{\bar{\alpha}}(\alpha)$] is the marginal pdf of τ [resp. α] and $\bar{g}_{\bar{\tau}|\bar{\alpha}}(\tau|\alpha)$ [resp., $\bar{g}_{\bar{\alpha}|\bar{\tau}}(\alpha|\tau)$] is the conditional pdf of τ given α [resp., α given τ]. The two identities in (49) and (50) suggest the following two respective alternatives to generate the required realizations:

(1) ALTERNATIVE 1: generate $\tau_q^{(r)}$ using $\bar{g}_{\bar{\tau}}(\tau)$ and then use $\bar{g}_{\bar{\alpha}|\bar{\tau}}(\alpha|\tau = \tau_q^{(r)})$ to generate $\alpha_q^{(r)}$.
(2) ALTERNATIVE 2: generate $\alpha_q^{(r)}$ using $\bar{g}_{\bar{\alpha}}(\alpha)$ and then use $\bar{g}_{\bar{\tau}|\bar{\alpha}}(\tau|\alpha = \alpha_q^{(r)})$ to generate $\tau_q^{(r)}$.
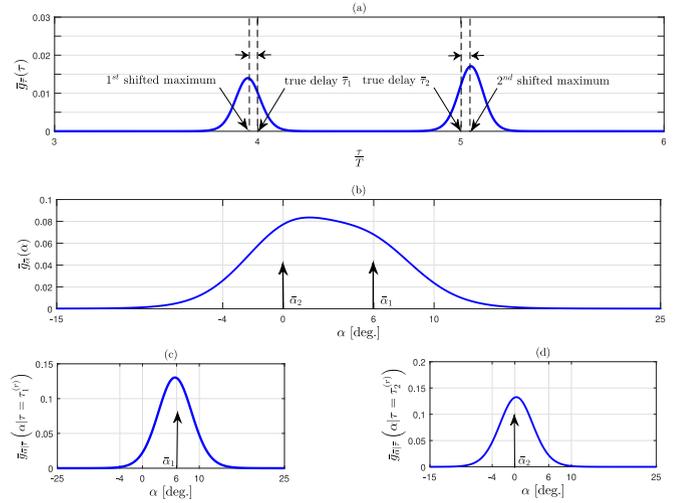

Fig. 2. Marginal and conditional pdfs illustrated in a single-carrier system, ULA, $P = 5$, $\bar{Q} = 2$ and SNR = 30 dB: (a) Marginal pdf of τ, (b) marginal pdf of α, (c) conditional pdf of α given $\tau_1^{(r)}$, and (d) conditional pdf of α given $\tau_2^{(r)}$.

In practice, however, "ALTERNATIVE 2", is not a good option since $\bar{g}_{\bar{\alpha}}(\alpha)$ cannot allow resolution of closely-spaced angles inevitably embodied by a single main lobe even in the total absence of noise. Fig. 2b illustrates this phenomenon in single-carrier systems for a modulated signal (with symbol duration T) propagating via two paths with delays $\bar{\tau}_1 = 4T$ and $\bar{\tau}_2 = 5T$ and angular separation $|\bar{\alpha}_1 - \bar{\alpha}_2| = 6°$.

In contrast, it is found that $\bar{g}_{\bar{\tau}}(\tau)$ always exhibits $\bar{Q}$ main lobes around the true unknown TDs, $\{\bar{\tau}_q\}_{q=1}^{\bar{Q}}$, even if the latter are associated to closely-spaced angles as depicted in Fig. 2a. Moreover, as will be seen in Section 8, $\bar{g}_{\bar{\tau}}(\tau)$ is able to resolve closely-spaced delays even if the two paths are also *extremely* closely spaced in the angular domain (typically, $|\bar{\alpha}_1 - \bar{\alpha}_2| = 0.5°$). For these reasons, we opt for "ALTERNATIVE 1" and first evaluate $\bar{g}_{\bar{\tau}}(\tau)$ as follows:

$$\bar{g}_{\bar{\tau}}(\tau) = \int \bar{g}_{\bar{\alpha},\bar{\tau}}(\alpha, \tau)d\alpha, \qquad (51)$$

which is then used to generate the rth vector of delay realizations, $\boldsymbol{\tau}^{(r)} = \left[\tau_1^{(r)}, \tau_2^{(r)}, \ldots, \tau_{\bar{Q}}^{(r)}\right]^T$, as will be explained shortly. Now, for the same angular separation (i.e., $|\alpha_1 - \alpha_2| = 6°$) and as depicted in Figs. 2c and 2d, each $\{q^{th}\}_{q=1}^{\bar{Q}}$ conditional angle pdf

$$\bar{g}_{\bar{\alpha}|\bar{\tau}}(\alpha|\tau = \tau_q^{(r)}) = \frac{\bar{g}_{\bar{\alpha},\bar{\tau}}(\alpha, \tau_q^{(r)})}{\bar{g}_{\bar{\tau}}(\tau_q^{(r)})}, \qquad (52)$$

is found to exhibit exactly a single main lobe around the true angle $\bar{\alpha}_q$ associated to $\bar{\tau}_q$. Next, we recall the following lemma [35] that will be used to generate the required realizations:

Lemma 1. *Let* $X \in \mathcal{X}$ *be any RV with pdf* $f_X(x)$ *and CDF* $F_X(x)$ *and denote the inverse CDF as* $F_X^{-1}(.) : [0, 1] \longrightarrow \mathcal{X}$, $u \longmapsto x$ *s.t.* $F_X(x) = u$. *Then, for any uniform RV,* $U \in [0, 1]$, *the RV* $\tilde{X} = F_X^{-1}(U)$ *is distributed according to* $f_X(.)$.

In principle, $\bar{g}_{\bar{\tau}}(\tau)$ can be used along with the result of LEMMA 1 to generate the required delay realizations $\{\tau_q^{(r)}\}_{r=1}^{R} \sim \bar{g}_{\bar{\tau}}(\tau)$ for every $q = 1, 2, \ldots, \bar{Q}$ as follows:
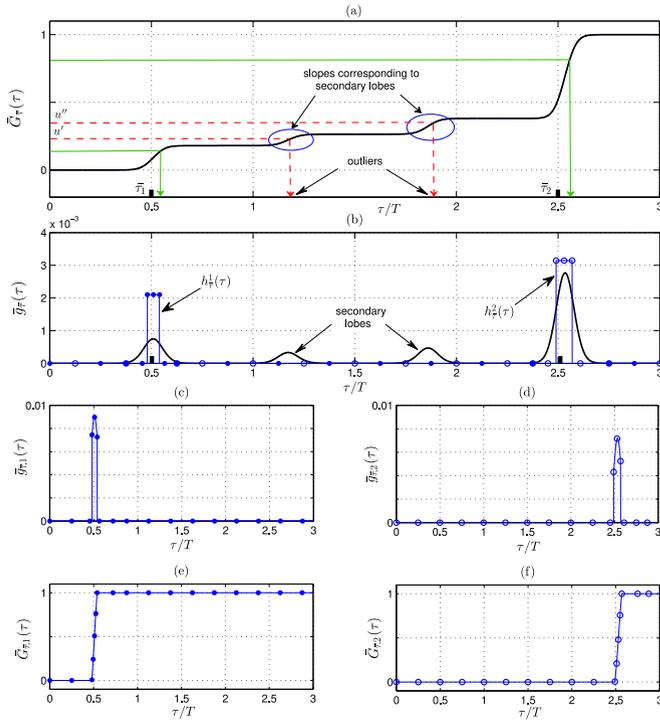
Fig. 3. Pseudo-pdfs in a single-carrier system illustrated for $\bar{Q} = 2$ and SNR = -5 dB: (a) Marginal CDF of τ, (b) marginal pdf of τ, (c) local pdf of τ around $\bar{\tau}_1$, (d) local pdf of τ around $\bar{\tau}_2$, (e) local CDF of τ around $\bar{\tau}_1$, and (f) local CDF of τ around $\bar{\tau}_2$.

(1)   Generate R realizations $\{u_q^{(r)}\}_{r=1}^R \sim U[0, 1]$,

(2)   Obtain $\tau_q^{(r)} = \bar{G}_{\bar{\tau}}^{-1}(u_q^{(r)})$ where $\bar{G}_{\bar{\tau}}(.)$ is the CDF associated to $\bar{g}_{\bar{\tau}}(\tau)$.

However, depending on the SNR level, the direct use of the marginal pdf $\bar{g}_{\bar{\tau}}(\tau)$ faces the following major problems in practice:

- At low SNR levels, $\bar{g}_{\bar{\tau}}(\tau)$ exhibits non-negligible secondary lobes, as depicted in Fig. 3b with SNR = -5 dB, which translate into spurious slopes in the CDF, $\bar{G}_{\bar{\tau}}(\tau)$, as seen from Fig. 3a. Consequently, any realization $u \sim U[0, 1]$ that falls within the range of such spurious slopes (along the y-axis) will result in a delay realization $\tau = \bar{G}_{\bar{\tau}}^{-1}(u)$ that does not correspond to any of the true delays (i.e., an *outlier*). This phenomenon is also illustrated in Fig. 3a for the two typical realizations u' and u''. Such outliers affect severely the performance of the estimator. In order to obtain *outliers-free* realizations, it is possible to rid $\bar{g}_{\bar{\tau}}(\tau)$ from its secondary lobes by choosing a sufficiently large value for the design parameter ρ_1 [cf. (42)]. Taking a large value for ρ_1, however, renders the main lobes in $\bar{g}_{\bar{\tau}}(\tau)$ extremely narrow making it more likely that the true delays lie outside their very short spans. Consequently, all the *outliers-free* realizations will be shifted, thereby resulting in an inevitable estimation bias.

- At sufficiently high SNR levels, however, the secondary lobes are naturally absent and thus a small value for ρ_1 can be chosen. Yet, the difference in main lobes' sizes results in out-of-proportion slopes in the CDF. As such, an unbalanced number of realizations will be generated under the different main lobes. As a brute-force remedy, one could be tempted by

choosing an extremely large value of R to guarantee that a sufficient number of realizations be generated under each main lobe; not without having to pay a significant extra cost in terms of increased complexity though.

To sidestep all the aforementioned problems, we describe hereafter a simple procedure that allows one to generate all the realizations around the true delays and angles thereby avoiding systematically the problem of outliers. Moreover, it ensures that the realizations are generated in exactly the same number under each of the main lobes irrespectively of their relative sizes. To do so, we begin by extracting—through a broad line search—some initial estimates of the unknown true TDs as follows:

$$[\widehat{\bar{\tau}}_1^{(0)}, \widehat{\bar{\tau}}_2^{(0)}, \ldots, \widehat{\bar{\tau}}_{\bar{Q}}^{(0)}] = \text{argmax}_{\bar{Q}} \ \bar{g}_{\bar{\tau}}(\tau), \quad (53)$$

where $\text{argmax}_{\bar{Q}}\{.\}$ returns the positions of the $\bar{Q}$ largest peaks of any objective function. This initial broad line search is performed using a relatively large grid step $\Delta_{\bar{\tau}}$. Since the main lobes of $\bar{g}_{\bar{\tau}}(\tau)$ are shifted [cf. Fig. 2a], note that (53) does not provide the delay MLEs even by taking an arbitrarily small value for $\Delta_{\bar{\tau}}$. Then, initial estimates for the associated AoAs are obtained as

$$\widehat{\bar{\alpha}}_q^{(0)} = \text{argmax}_{\alpha} \ \bar{g}_{\bar{\alpha}|\bar{\tau}}\left(\alpha|\tau = \widehat{\bar{\tau}}_q^{(0)}\right), \quad q = 1, \ldots, \bar{Q}. \quad (54)$$

Likewise, the initial line search in (54) is performed with a large grid step $\Delta_{\bar{\alpha}}$. To force $\{\tau_q^{(r)}\}_{r=1}^R$ and $\{\alpha_q^{(r)}\}_{r=1}^R$ to be generated in the vicinity of $\bar{\tau}_q$ and $\bar{\alpha}_q$, respectively, we fix the following $\bar{Q}$ local intervals

$$D_{\widehat{\bar{\tau}}_q^{(0)}} = \left[\widehat{\bar{\tau}}_q^{(0)} - \delta_{\bar{\tau}}, \ \widehat{\bar{\tau}}_q^{(0)} + \delta_{\bar{\tau}}\right],$$

$$D_{\widehat{\bar{\alpha}}_q^{(0)}} = \left[\widehat{\bar{\alpha}}_q^{(0)} - \delta_{\bar{\alpha}}, \ \widehat{\bar{\alpha}}_q^{(0)} + \delta_{\bar{\alpha}}\right],$$

which are centered at $\widehat{\bar{\tau}}_q^{(0)}$ and $\widehat{\bar{\alpha}}_q^{(0)}$. The sizes of such local delay and angle intervals are governed by the design parameters $\delta_{\bar{\tau}}$ and $\delta_{\bar{\alpha}}$ whose values will be specified in Section 8. We also define the associated delay and angle *impulse* functions as follows:

$$h_{\widehat{\bar{\tau}}_q^{(0)}}(\tau) = \begin{cases} h_{\bar{\tau}}^q & \text{for } \tau \in D_{\widehat{\bar{\tau}}_q^{(0)}}, \\ 0 & \text{otherwise;} \end{cases} \quad (55)$$

$$h_{\widehat{\bar{\alpha}}_q^{(0)}}(\alpha) = \begin{cases} h_{\bar{\alpha}}^q & \text{for } \alpha \in D_{\widehat{\bar{\alpha}}_q^{(0)}}, \\ 0 & \text{otherwise;} \end{cases} \quad (56)$$

In the specific case of $\bar{Q} = 2$, the two delay *impulse* functions are illustrated in Fig. 3b with dotted and circled lines. The qth delay and angle pseudo-pdfs (referred to hereafter as *local* pseudo-pdfs) that will be used to generate the realizations in $D_{\widehat{\bar{\tau}}_q^{(0)}} \times D_{\widehat{\bar{\alpha}}_q^{(0)}}$ are given by

$$\bar{g}_{\bar{\tau},q}(\tau) = h_{\bar{\tau}}^q(\tau)\bar{g}_{\bar{\tau}}(\tau), \quad (57)$$

$$\bar{g}_{\bar{\alpha}|\bar{\tau},q}(\alpha|\tau) = h_{\bar{\alpha}}^q(\alpha)\bar{g}_{\bar{\alpha}|\bar{\tau}}(\alpha|\tau), \quad (58)$$

for $q = 1, 2, \ldots, \bar{Q}$. The constants $h_{\bar{\tau}}^q$ and $h_{\bar{\alpha}}^q$ in (55) and (56) are computed such that the local pseudo-pdfs in (57) and (58) sum up to one thereby yielding

$$h_{\bar{\tau}}^q = \left(\int_{\hat{\bar{\tau}}_q^{(0)} - \delta_{\bar{\tau}}}^{\hat{\bar{\tau}}_q^{(0)} + \delta_{\bar{\tau}}} \bar{g}_{\bar{\tau}}(\tau) d\tau \right)^{-1}. \tag{59}$$

$$h_{\bar{\alpha}}^q = \left(\int_{\hat{\bar{\alpha}}_q^{(0)} - \delta_{\bar{\alpha}}}^{\hat{\bar{\alpha}}_q^{(0)} + \delta_{\bar{\alpha}}} \bar{g}_{\bar{\alpha}|\bar{\tau}}(\alpha|\tau) d\alpha \right)^{-1}. \tag{60}$$

Note here that by applying the impulse functions in (57) and (58) we obtain a separate (i.e., isolated) local angle/delay pseudo-pdf for each qth path. Therefore, in practice, the processes of generating the required realizations locally around each true delay/angle couple, $(\bar{\alpha}_q, \bar{\tau}_q)$, can be implemented separately and run in parallel with a much faster and less complex execution.

For better illustration, the isolated local delay pseudo-pdfs, $\bar{g}_{\bar{\tau},1}(\tau)$ and $\bar{g}_{\bar{\tau},2}(\tau)$, in the specific case of $\bar{Q} = 2$ are depicted in Figs. 3c and 3d, respectively. Further, as seen from Figs. 3e and 3f, the associated local CDFs, $\bar{G}_{\bar{\tau},1}(\tau)$ and $\bar{G}_{\bar{\tau},2}(\tau)$, exhibit a single slope that is located around the corresponding true delay. Therefore, by applying the result of Lemma 1, every uniform realization $u_q^{(r)} \in [0,1]$ will yield a delay realization $\tau_q^{(r)} \in D_{\hat{\bar{\tau}}_q^{(0)}}$ [i.e., in the vicinity of $\bar{\tau}_q$]. For the same reasons, all the angle realizations that are generated using the qth isolated conditional pdfs fall in in the vicinity of $\bar{\alpha}_q$.

8 IMPLEMENTATION DETAILS

8.1 Local Generation of the Required Realizations

In this section, we give all the necessary details for an easy and practical implementation of the newly proposed IS-based ML JADE algorithm. Without loss of generality, we consider the case of a ULA with $\alpha = 0$ corresponding to the broadside axis. Hence, the candidate angles are confined within $[-\pi/2, \pi/2]$ and recall that $\tau \in [0, \bar{\tau}_{\max}]$ where $\bar{\tau}_{\max}$ can be freely chosen as high as desired. The starting point of the algorithm is the evaluation of the periodogram, $I(\alpha_i, \tau_j)$ at multiple grid points (α_i, τ_j) with relatively large discretization steps $\Delta_{\bar{\alpha}}^{\text{broad}}$ and $\Delta_{\bar{\tau}}^{\text{broad}}$. Then, by approximating integrals with discrete sums, we evaluate the joint pdf in (42), $\bar{g}_{\bar{\alpha},\bar{\tau}}(\alpha, \tau)$, at every grid point (i.e., $\forall (\alpha_i, \tau_j) \in [-\pi/2, \pi/2] \times [0, \bar{\tau}_{\max}]$) as follows:

$$\bar{g}_{\bar{\alpha},\bar{\tau}}(\alpha_i, \tau_j) = \frac{\exp\{\rho_1 I(\alpha_i, \tau_j)\}}{\sum_i \sum_j \exp\{\rho_1 I(\alpha_i, \tau_j)\} \Delta_{\bar{\tau}}^{\text{broad}} \Delta_{\bar{\alpha}}^{\text{broad}}}, \tag{61}$$

from which the marginal delay pdf is computed as follows:

$$\bar{g}_{\bar{\tau}}(\tau_j) = \sum_i \bar{g}(\alpha_i, \tau_j) \Delta_{\bar{\alpha}}^{\text{broad}}, \qquad \forall \tau_j \in [0, \tau_{\max}]. \tag{62}$$

The initial delay estimates, $\{\hat{\bar{\tau}}_q^{(0)}\}_{q=1}^{\bar{Q}}$, are the discrete delay points that correspond to the largest $\bar{Q}$ maxima of (62). Then, for every $q = 1, 2, \ldots, \bar{Q}$, the conditional pdf of the qth angle corresponding to $\hat{\bar{\tau}}_q^{(0)}$ is directly obtained as

$$\bar{g}_{\bar{\alpha}|\bar{\tau}}\left(\alpha_i | \tau = \hat{\bar{\tau}}_q^{(0)}\right) = \frac{\bar{g}_{\bar{\alpha},\bar{\tau}}\left(\alpha_i, \hat{\bar{\tau}}_q^{(0)}\right)}{\bar{g}_{\bar{\tau}}(\hat{\bar{\tau}}_q^{(0)})}, \quad \forall \alpha_i \in \left[-\frac{\pi}{2}, \frac{\pi}{2}\right]. \tag{63}$$

The initial estimate, $\hat{\bar{\alpha}}_q^{(0)}$, for the qth AoA is the discrete point, α_i, that corresponds to the maximum of (63). Then, the process of generating the realizations in the intervals $D_{\hat{\bar{\tau}}_q^{(0)}}$ and $D_{\hat{\bar{\alpha}}_q^{(0)}}$ amounts to performing the following steps for every $q = 1, 2, \ldots \bar{Q}$:

- STEP 1: Evaluate the joint pdf, $\bar{g}_{\bar{\alpha},\bar{\tau}}(\alpha, \tau)$, *locally* at new discrete points $(\alpha_i', \tau_j') \in D_{\hat{\bar{\alpha}}_q^{(0)}} \times D_{\hat{\bar{\tau}}_q^{(0)}}$ as in (61); yet with smaller grid steps $\Delta_{\bar{\tau}}^{\text{small}} < \Delta_{\bar{\tau}}^{\text{broad}}$ and $\Delta_{\bar{\alpha}}^{\text{small}} < \Delta_{\bar{\alpha}}^{\text{broad}}$.

- STEP 2: Compute the qth local marginal delay pdf at every point $\tau_j' \in D_{\hat{\bar{\tau}}_q^{(0)}}$ as in (62), i.e.,

$$\bar{g}_{\bar{\tau},q}(\tau_j') = \sum_i \bar{g}(\alpha_i', \tau_j') \Delta_{\bar{\alpha}}^{\text{small}} \quad \forall \tau_j' \in D_{\hat{\bar{\tau}}_q^{(0)}}. \tag{64}$$

- STEP 3: Compute the qth local delay CDF as follows:

$$\bar{G}_{\bar{\tau},q}(\tau_j') = \sum_{l \le j} \bar{g}_{\bar{\tau},q}(\tau_l') \Delta_{\bar{\tau}}^{\text{small}} \quad \forall \tau_j' \in D_{\hat{\bar{\tau}}_q^{(0)}}. \tag{65}$$

- STEP 4: Generate R realizations $\{u_q^{(r)}\}_{r=1}^R \sim U[0,1]$ and invert $\bar{G}_{\bar{\tau},q}(.)$ via linear interpolation in order to obtain the local delay realizations $\tau_q^{(r)} = \bar{G}_{\bar{\tau},q}^{-1}(u_q^{(r)})$ for $r = 1, 2 \ldots R$.

- STEP 5: For $r = 1, 2, \ldots, R$, obtain immediately the local pdf of the qth AoA conditioned on $\tau_q^{(r)}$ from the local joint pdf (already evaluated in "STEP 1") as follows:

$$\bar{g}_{\bar{\alpha}|\bar{\tau}}\left(\alpha_i' | \tau = \tau_q^{(r)}\right) = \frac{\bar{g}_{\bar{\alpha},\bar{\tau}}\left(\alpha_i', \tau_q^{(r)}\right)}{\bar{g}_{\bar{\tau},q}\left(\tau_q^{(r)}\right)}, \quad \forall \alpha_i' \in D_{\hat{\bar{\alpha}}_q^{(0)}}.$$

- STEP 6: Evaluate the qth local angle CDF, $\bar{G}_{\bar{\alpha},q}(\alpha_i')$, similarly to $\bar{G}_{\bar{\tau},q}(\tau_j')$ in (65) and generate the rth angle realization, $\alpha_q^{(r)} = \bar{G}_{\bar{\alpha},q}^{-1}(u_q^{(r)})$, using linear interpolation as well.

8.2 Estimations of the TDs and AoAs

Using the same arguments of [15], [25], after generating all the required realizations, more accurate IS-based parameter estimates are obtained by applying the *circular* instead of the *linear* sample mean estimate. In fact, the latter simply averages out all the realizations and outlier seeds will result in an inevitable estimation bias. As will be shown later in this paper, however, the circular mean succeeds in selecting the best angle and delay realizations in terms of Euclidean distance to the true multipath-resolution parameters. The circular mean [39, ch. 2,3] of any transformation $f(\Phi)$ of a given random variable $\Phi \in [-\pi, \pi]$ with distribution $p_\Phi(\phi)$ is obtained as follows:

$$\hat{\bar{\phi}} = \angle \frac{1}{R} \sum_{r=1}^R f(\phi^{(r)}) e^{j\phi^{(r)}}, \tag{66}$$

where $\phi^{(r)} \sim p_\Phi(.)$ are R realizations of Φ. Note here that the original realizations $\tau_q^{(r)}$ and $\alpha_q^{(r)}$ are, respectively, in $[0, \tau_{\max}]$ and $[-\pi/2, \pi/2]$ for ULAs ($[0, 2\pi]$ for UCAs). Therefore, one needs to transform both of them into the interval $[-\pi, \pi]$ in order to successfully apply the circular mean. To that end, we use the transformations $\phi_1(\tau_q^{(r)}) = 2\pi(\tau_q^{(r)}/\tau_{\max} - 1/2) \in [-\pi, \pi]$ and $\phi_2(\alpha_q^{(r)}) = 2\alpha_q^{(r)} \in [-\pi, \pi]$ for ULAs.[4] The circular mean is first applied using $\phi_1(\tau_q^{(r)})$ and $\phi_2(\alpha_q^{(r)})$ and the true TDs and AoAs are then estimated using the inverse

---

4. Note here that we will keep presenting the AoA estimates for ULA configurations and the results for UCAs are quite similar. The only difference is that the corresponding transformation is $\phi_2(\alpha_q^{(r)}) = \alpha_q^{(r)} - \pi$ and its inverse in (68) is $\phi_2^{-1}(x) = x + \pi$.

transformations $\phi_1^{-1}(x) = \tau_{\max}\left(\frac{1}{2} + \frac{1}{2\pi}x\right)$ and $\phi_2^{-1}(x) = \frac{1}{2}x$ as follows:

$$\widehat{\overline{\tau}}_q = \tau_{\max}\left(\frac{1}{2\pi}\angle\left[\sum_{r=1}^{R}\eta(\boldsymbol{\alpha}^{(r)}, \boldsymbol{\tau}^{(r)})e^{j2\pi\left(\frac{\tau_q^{(r)}}{\tau_{\max}} - \frac{1}{2}\right)}\right] + \frac{1}{2}\right), \quad (67)$$

$$\widehat{\overline{\alpha}}_q = \frac{1}{2}\angle\left[\sum_{r=1}^{R}\eta(\boldsymbol{\alpha}^{(r)}, \boldsymbol{\tau}^{(r)})e^{j\left(2\alpha_q^{(r)} - \pi\right)}\right]. \quad (68)$$

Now by using (17) and (40) in (24), the weighting coefficient $\eta(\boldsymbol{\alpha}^{(r)}, \boldsymbol{\tau}^{(r)})$ can be explicitly expressed as follows:

$$\eta(\boldsymbol{\alpha}^{(r)}, \boldsymbol{\tau}^{(r)}) = \frac{\mu\,\exp\left\{\rho_0\mathcal{L}_c(\boldsymbol{\alpha}^{(r)}, \boldsymbol{\tau}^{(r)})\right\}}{\exp\left\{\rho_1\sum_{q=1}^{\bar{Q}}I(\alpha_q^{(r)}, \tau_q^{(r)})\right\}}, \quad (69)$$

where

$$\mu = \frac{\int\cdots\int\exp\left\{\rho_1\sum_{q=1}^{\bar{Q}}I(\alpha_q, \tau_q)\right\}d\boldsymbol{\alpha}d\boldsymbol{\tau}}{\int\cdots\int\exp\{\rho_0\mathcal{L}_c(\boldsymbol{\alpha}, \boldsymbol{\tau})\}d\boldsymbol{\alpha}d\boldsymbol{\tau}}. \quad (70)$$

Actually, by defining the quantity

$$\Psi(\boldsymbol{\alpha}, \boldsymbol{\tau}) \triangleq \rho_0\mathcal{L}_c(\boldsymbol{\alpha}, \boldsymbol{\tau}) - \rho_1\sum_{q=1}^{\bar{Q}}I(\alpha_q, \tau_q), \quad (71)$$

and using the same arguments in [15], one can use the following *normalized* weighting coefficient

$$\overline{\eta}(\boldsymbol{\alpha}^{(r)}, \boldsymbol{\tau}^{(r)}) = \exp\left\{\Psi(\boldsymbol{\alpha}^{(r)}, \boldsymbol{\tau}^{(r)}) - \max_{1\leq r\leq R}\Psi(\boldsymbol{\alpha}^{(r)}, \boldsymbol{\tau}^{(r)})\right\}, \quad (72)$$

instead of $\eta(\boldsymbol{\tau}^{(r)}, \boldsymbol{\alpha}^{(r)})$ in order to greatly reduce the computational load with no changes in the final results. Actually we further show in this paper the following interesting result:

Lemma 2. *The circular-mean estimates, $\widehat{\overline{\boldsymbol{\tau}}} = [\widehat{\overline{\tau}}_1, \widehat{\overline{\tau}}_2, \ldots, \widehat{\overline{\tau}}_{\bar{Q}}]$ and $\widehat{\overline{\boldsymbol{\alpha}}} = [\widehat{\overline{\alpha}}_1, \widehat{\overline{\alpha}}_2, \ldots, \widehat{\overline{\alpha}}_{\bar{Q}}]$, obtained in (67) and (68) by using the normalized factor in (72) correspond to the vector realizations that jointly minimize the Euclidean distance to the true delay and angle parameters, i.e.,*

$$\left[\widehat{\overline{\boldsymbol{\tau}}}, \widehat{\overline{\boldsymbol{\alpha}}}\right] = \arg\min_{\boldsymbol{\tau}^{(r)}, \boldsymbol{\alpha}^{(r)}}\left(\left||\boldsymbol{\tau}^{(r)} - \overline{\boldsymbol{\tau}}||\right|^2 + \left||\boldsymbol{\alpha}^{(r)} - \overline{\boldsymbol{\alpha}}||\right|^2\right). \quad (73)$$

Proof. See Appendix A, which can be found on the Computer Society Digital Library at http://doi.ieeecomputersociety.org/10.1109/TMC.2018.2854883. □

In the sequel, we shall suggest other tricks that result in tremendous additional computational savings and make the proposed estimator always reach the CRLB. In fact, it is found that the initial estimates $\widehat{\overline{\tau}}_q^{(0)}$ and $\widehat{\overline{\alpha}}_q^{(0)}$ are shifted, respectively, by at most ϵ_τ and ϵ_α from the true delays and angles[5] (i.e., $|\widehat{\overline{\tau}}_q^{(0)} - \overline{\tau}_q| \leq \epsilon_\tau$ and $|\widehat{\overline{\alpha}}_q^{(0)} - \overline{\alpha}_q| \leq \epsilon_\alpha$). In principle, the IS-based estimates in (67) and (68) are able to return the exact (non-shifted) MLEs by using an extremely large number of realizations. Indeed, using exhaustive simulations, it

was found that the exact MLEs are obtained with $R_0 = 20000$ realizations that are generated locally using $\delta_{\bar{\tau}} = 2\epsilon_\tau$ and $\delta_{\bar{\alpha}} = 2\epsilon_\alpha$. These typical values for $\delta_{\bar{\tau}}$ and $\delta_{\bar{\alpha}}$ are chosen so that the corresponding local intervals $D_{\widehat{\overline{\tau}}_q^{(0)}} = \left[\widehat{\overline{\tau}}_q^{(0)} - \delta_{\bar{\tau}}, \widehat{\overline{\tau}}_q^{(0)} + \delta_{\bar{\tau}}\right]$ and $D_{\widehat{\overline{\alpha}}_q^{(0)}} = \left[\widehat{\overline{\alpha}}_q^{(0)} - \delta_{\bar{\alpha}}, \widehat{\overline{\alpha}}_q^{(0)} + \delta_{\bar{\alpha}}\right]$ include the true values of the unknown parameters since they verify $|\widehat{\overline{\tau}}_q^{(0)} - \overline{\tau}_q| \leq \delta_{\bar{\tau}}/2$ and $|\widehat{\overline{\alpha}}_q^{(0)} - \overline{\alpha}_q| \leq \delta_{\bar{\alpha}}/2$. This ensures that a portion of the $R_0 = 20000$ realizations are indeed generated on both sides of each true TD and AoA as required by the IS concept. However, using such a very large number of realizations results in a very high computational load. In order to greatly reduce complexity, the algorithm is run in a two-stage[6] multi-resolution implementation where, in each stage, a far smaller number of realizations is generated over a far narrower lock span around the target parameters.

- STAGE I: Generate $R_1 \ll R_0$ realizations, $\{\tau_q^{(r)}\}_{r=1}^{R_1}$ and $\{\alpha_q^{(r)}\}_{r=1}^{R_1}$, in the aforementioned local intervals $D_{\widehat{\overline{\tau}}_q^{(0)}}$ and $D_{\widehat{\overline{\alpha}}_q^{(0)}}$ and obtain the estimates $\widehat{\overline{\tau}}_q$ and $\widehat{\overline{\alpha}}_q$ as in (67) and (68).

- STAGE II: Regenerate $R_2 \ll R_0$ new realizations $\{\tau_q'^{(r)}\}_{r=1}^{R_2}$ and $\{\alpha_q'^{(r)}\}_{r=1}^{R_2}$ over narrower intervals that are centered around the estimates $\widehat{\overline{\tau}}_q$ and $\widehat{\overline{\alpha}}_q$ obtained in "STAGE I", i.e., $D'_{\widehat{\overline{\tau}}_q} = [\widehat{\overline{\tau}}_q - \delta'_{\bar{\tau}}, \widehat{\overline{\tau}}_q + \delta'_{\bar{\tau}}]$ and $D'_{\widehat{\overline{\alpha}}_q} = [\widehat{\overline{\alpha}}_q - \delta'_{\bar{\alpha}}, \widehat{\overline{\alpha}}_q + \delta'_{\bar{\alpha}}]$ with $\delta'_{\bar{\tau}} = \delta_{\bar{\tau}}/10$ and $\delta'_{\bar{\alpha}} = \delta_{\bar{\alpha}}/10$. Then, compute the AoA MLEs using the new angle realizations, $\{\boldsymbol{\alpha}'^{(r)} = [\alpha_1'^{(r)}, \alpha_2'^{(r)}, \ldots, \alpha_{\bar{Q}}'^{(r)}]\}_{r=1}^{R_2}$, and the delay estimates, $\widehat{\overline{\boldsymbol{\tau}}} = [\widehat{\overline{\tau}}_1, \widehat{\overline{\tau}}_2, \ldots, \widehat{\overline{\tau}}_{\bar{Q}}]^T$, obtained in "STAGE I" as follows:

$$\widehat{\overline{\alpha}}_{q,\,\text{MLE}} = \frac{1}{2}\angle\left[\sum_{r=1}^{R_2}\overline{\eta}(\boldsymbol{\alpha}'^{(r)}, \widehat{\overline{\boldsymbol{\tau}}})e^{j\left(2\alpha_q'^{(r)} - \pi\right)}\right]. \quad (74)$$

All the AoA MLEs obtained in (74), i.e., $\widehat{\overline{\boldsymbol{\alpha}}}_{\text{MLE}} = [\widehat{\overline{\alpha}}_{1,\text{MLE}}, \widehat{\overline{\alpha}}_{2,\text{MLE}}, \ldots, \widehat{\overline{\alpha}}_{\bar{Q},\text{MLE}}]^T$, are then used in conjunction with the new delay realizations, $\{\boldsymbol{\tau}'^{(r)} = [\tau_1'^{(r)}, \tau_2'^{(r)}, \ldots, \tau_{\bar{Q}}'^{(r)}]\}_{r=1}^{R_2}$, to find the TD MLEs as follows:

$$\widehat{\overline{\tau}}_{q,\,\text{MLE}} = \tau_{\max}\left(\frac{1}{2\pi}\angle\left[\sum_{r=1}^{R_2}\overline{\eta}(\boldsymbol{\tau}'^{(r)}, \widehat{\overline{\boldsymbol{\alpha}}}_{\text{MLE}})e^{j2\pi\left(\frac{\tau_q'^{(r)}}{\tau_{\max}} - \frac{1}{2}\right)}\right] + \frac{1}{2}\right). \quad (75)$$

Finally, we emphasize the fact that the generated angle and delay realizations are not constrained to be on the grid points due to the use of the linear interpolation in "STEP 4" and "STEP 6". Therefore, unlike all the existing JADE estimators, the new IS-based ML technique does not suffer from the *off-grid* problems as the MLEs obtained in (74) and (75) are not also constrained to be on the considered sampling grid (cf. Section 1 for more details).

9 ESTIMATING THE NUMBER OF PATHS

All the existing JADE techniques as well as the new IS-based one require the *a priori* knowledge of the number of paths $\bar{Q}$. In practice, however, this parameter is also

---

5. Note here that ϵ_τ and ϵ_α depend on the bandwith of the known transmitted signal and their expressions will be given later in Section 10 for both single- and multi-carrier systems.

6. An N-stage multi-resolution extension would be straightforward.

unknown and needs to be estimated even before proceeding to AoAs and TDs acquisition. In this contribution, we also propose a new heuristic approach that allows the exact estimation of $\bar{Q}$ over a wide range of practical SNRs. As will be seen shortly, the new approach is intrinsic to the new IS-based estimator and entails almost no additional complexity. In fact, it relies on the sparsity feature inherent to the marginal delay pdf, $\bar{g}_{\bar{\tau}}(\tau_i)$, depicted in Fig. 3b. Indeed, by properly selecting the *sparsity-promoting* design parameter ρ_1, it is possible to reduce the sizes of the secondary lobes that are due to the noise contribution. In this way, one obtains a pseudo-pdf whose energy is almost totally concentrated under the main lobes that are located around the true delays. Precisely, just after evaluating $\bar{g}_{\bar{\tau}}(\tau_i)$ in (62) over $[0, \tau_{\max}]$, the following two simple steps are performed:

(1)   STEP 1: Get the points, $\{\mathring{\tau}_q\}_q^{Q_{\text{tot.}}}$, corresponding to all the peaks in $\{\bar{g}_{\bar{\tau}}(\tau_i) \, \forall \tau_i \in [0, \tau_{\max}]\}$ with $Q_{\text{tot.}}$ being the total number of peaks. Note here that $Q_{\text{tot.}}$ is always greater than $\bar{Q}$ due to the presence of secondary lobes.

(2)   STEP 2: Sort the squared magnitudes, $\{|\bar{g}_{\bar{\tau}}(\mathring{\tau}_q)|^2\}_q^{Q_{\text{tot.}}}$ corresponding to $\{\mathring{\tau}_q\}_q^{Q_{\text{tot.}}}$ and obtain an estimate, $\widetilde{\bar{Q}}$ (for the actual number of paths) as the first number of peaks, Q, whose combined energy fractions is above a certain threshold, i.e.,

$$\rho(Q) = \frac{\sum_q^Q |\bar{g}_{\bar{\tau}}(\mathring{\tau}_q)|^2}{\sum_q^{Q_{\text{tot.}}} |\bar{g}_{\bar{\tau}}(\mathring{\tau}_q)|^2} \geq \kappa, \qquad (76)$$

$$\rho(Q-1) = \frac{\sum_q^{Q-1} |\bar{g}_{\bar{\tau}}(\mathring{\tau}_q)|^2}{\sum_q^{Q_{\text{tot.}}} |\bar{g}_{\bar{\tau}}(\mathring{\tau}_q)|^2} < \kappa, \qquad (77)$$

where κ is some threshold level to be designed off-line as explained subsequently.

First, it is worth mentioning here that the procedure described above could not be deduced from any of the existing JADE estimators since none of them has a *sparsity-promoting* design parameter like our new IS-based estimator. In practice, they are hence compelled to use one of the traditional more complex signal detection schemes like [36] in order to estimate $\bar{Q}$.

As mentioned above, the threshold level, κ, can be easily optimized offline in order to obtain the lowest possible $\bar{Q}$-estimation error for all the practical values of $\bar{Q}$. To do so, for each $\bar{Q}$, the mean value of the ratio in (76), denoted here as $\bar{\rho}(Q) \triangleq \mathbb{E}\{\rho(Q)\}$, is evaluated by Monte-Carlo simulations for all $1 \leq Q \leq Q_{\text{tot.}}$. Then, the appropriate value for κ is selected based on these mean values as suggested by Fig. 4 (note here that Fig. 4b depicts a zoom of Fig. 4a around the specified region along the y-axis). These results are obtained from 10000 Monte-Carlo runs for every $\bar{Q}$ at an SNR $= -10$ dB.

As suggested by Fig. 4b, at such extremely low SNR level, an appropriate choice for the threshold level would be $\kappa = 0.96$. In fact, with such threshold, it is seen for $\bar{Q} = 2$ that the first value Q at which $\rho(Q)$ exceeds $\kappa = 0.96$ (on average) is $Q = 2$, i.e., "exact estimation". The same observation holds for $\bar{Q} = 3, 4, 5$ and 6 as seen from Fig. 4b. For $\bar{Q} = 7$, however, the first value Q that verifies (76) on average is $Q = 6$, i.e., "under-estimation" and the same observation holds as well for $\bar{Q} = 8$ and $\bar{Q} = 9$. It will be seen later that the proposed path detection technique outperforms the two well-known existing solutions, namely MDL and AIC
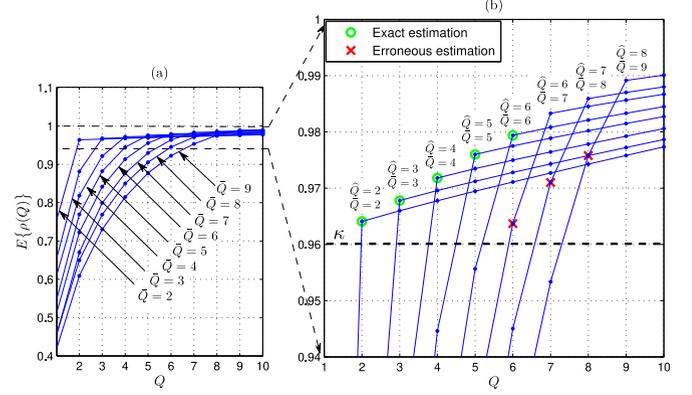

Fig. 4. The mean value of $\rho(Q)$ for different values of $\bar{Q}$, SNR $= -10$ dB, ULA with $P = 5$ receiving antennas.

[41], especially when the number of paths to be detected is larger then the number of receiving antennas.

10   SIMULATION RESULTS

10.1   Impact of Parameters ρ_0 and ρ_1

We first provide some hints about the appropriate choice of the parameters ρ_0 and ρ_1. We mention beforehand that (unlike ρ_0) ρ_1 is actually a design parameter that should be carefully chosen.

- Choice of ρ_0: As suggested by Pincus' theorem, the value of this parameter should be infinite so as to reflect the infinite limit involved in Pincus' theorem [23]. In practice, however, one needs to work with a finite yet sufficiently high value which is optimized offline depending on the observed behaviour of the estimator. In fact, it is found that for low values for ρ_0, the estimator exhibits very poor estimation performance as seen in Fig. 5 below for both single- and multi-carrier systems. By increasing ρ_0, the estimation accuracy improves remarkably. And starting from a lower threshold, $\bar{\rho}_0$, the performance holds the same; any value for $\rho_0 > \bar{\rho}_0$ can be used. As seen from Figs. 5a and 5b, the lower threshold on ρ_0 is found to be $\bar{\rho}_0 = 300$; above which the estimator performs well (i.e., close to the CRLB) both in terms of TDs and AoAs estimation.

- Choice of ρ_1: The main role of this design parameter is to control the spans of the main lobes in $\bar{g}_{\bar{\tau}}(\tau)$ and $\bar{g}_{\bar{\alpha}|\bar{\tau}}(\alpha|\tau)$ that appear, respectively, around the true (unknown) AoAs and TDs, $\{\bar{\alpha}_q\}_{q=1}^{\bar{Q}}$ and $\{\bar{\tau}_q\}_{q=1}^{\bar{Q}}$. Taking a large value for ρ_1 renders the main lobes in $\bar{g}_{\bar{\tau}}(\tau)$, for instance, extremely narrow making it more likely that the true delays lie outside their very short spans. Since the realizations pertaining to each qth delay, $\bar{\tau}_q$, are generated under the associated main lobe, they will be all shifted from $\bar{\tau}_q$ resulting in an inevitable estimation bias. Therefore, contrarily to ρ_o, there is an upper threshold, $\bar{\rho}_1$, that should not be exceeded by ρ_1 as shown in Fig. 6 below. There, we see that the upper threshold on ρ_1 is $\bar{\rho}_1 = 40$ as the performance of the estimator deteriorates greatly for $\rho_1 > 40$; especially in terms of delay estimation.

In Fig. 7, we gauge our proposed approach for estimating the number of paths, $\bar{Q}$, against the two widely used signal
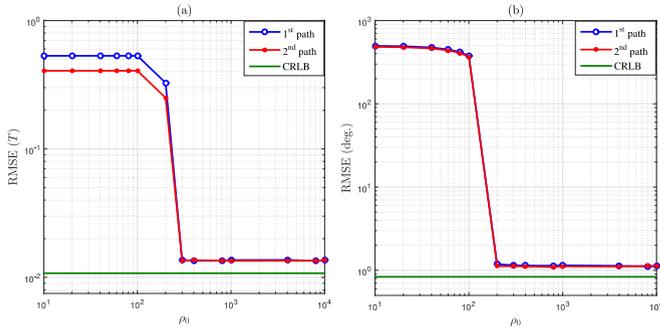
Fig. 5. Impact of the parameter, ρ_0, on the performance of the proposed IS-based estimator at SNR $= -10$ dB: (a) and (b) multi-carrier, $M = 244$, (c) and (d) single-carrier, $M = 128$.
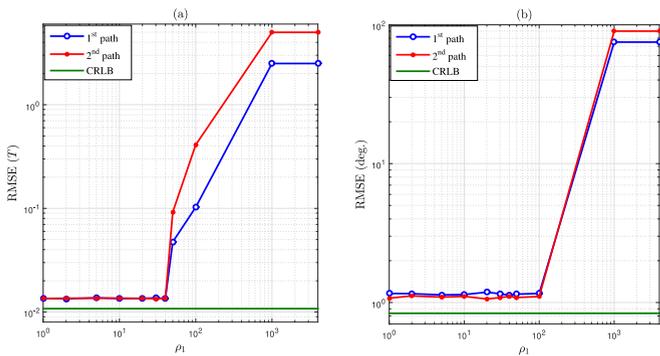

Fig. 6. Impact of the parameter, ρ_1, on the performance of the proposed IS-based estimator at SNR $= -10$ dB: (a) and (b) multi-carrier, $M = 244$, (c) and (d) single-carrier, $M = 128$.

detection schemes, namely MDL and AIC [41]. There, it is seen that the proposed approach outperforms both benchmarks in terms of the probability of detection error. This is mainly due to the use of the sparsity-promoting design parameter, ρ_1, whose appropriate selection allows to reduce the contributions of the spurious lobes stemming from the background noise. We emphasize, however, the fact that both MDL and AIC are applicable only when the actual number of paths, $\bar{Q}$, is smaller than the number of receiving antenna elements P since their cost functions can be evaluated for $1 \leq Q \leq P$ only.

In the remaining simulations, we assess the performance of the proposed IS-based ML estimator in terms of the root mean square error (RMSE) which is defined for each qth TD and AoA as follows:

$$\text{RMSE} = \sqrt{\frac{\sum_{m=1}^{M_c} \left(\widehat{\bar{\tau}}_{q,\,\text{MLE}}^{[m]} - \bar{\tau}_q \right)^2}{M_c}},$$

$$\text{RMSE}(\text{deg.}) = \sqrt{\frac{\sum_{m=1}^{M_c} \left(\widehat{\bar{\alpha}}_{q,\,\text{MLE}}^{[m]} - \bar{\alpha}_q \right)^2}{M_c}},$$

where $M_c = 5000$ is the total number of Monte-Carlo runs, in all simulations, and $\widehat{\bar{\tau}}_{q,\,\text{MLE}}^{[m]}$ and $\widehat{\bar{\alpha}}_{q,\,\text{MLE}}^{[m]}$ are, respectively, the estimates of $\bar{\tau}_q$ and $\bar{\alpha}_q$ during the mth Monte-Carlo run.

10.2 AoA and TD Estimation Accuracies: Multi-Carrier Case

We consider the IEEE 802.11ac standard's setup parameters with a bandwidth $B = 80$ MHz and $P = 6$ antenna elements. In this case, the subcarrier spacing is $\Delta F = 312.5$ KHz thereby leading to $M + 1 = 245$ useful subcarriers within
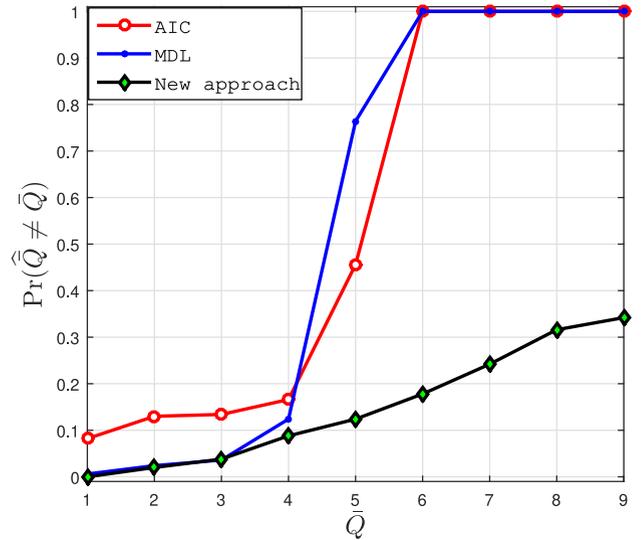

Fig. 7. Error probability on detecting the number of paths for a multicarrier-carrier system employing $M + 1 = 245$ subcarriers at SNR $= 0$ dB with $P = 5$ and $\rho_1 = 4$.

the considered bandwidth. According to the IEEE 802.11ac standard, there are 8 subcarriers allocated for other purposes that cannot be exploited for JADE. That is why we are left with only 245 useful subcarriers out of the 256 available in the considered setup.

10.2.1 MATLAB-Based Simulations

We will compare our estimator the unitary matrix pencil JADE algorithm introduced recently in [12], [13] and which remains so far the only technique that is geared specifically towards multicarrier systems. The two estimators will also be gauged against the CRLB developed in [13] and used here as an overall benchmark that reflects, for every considered setup, the best achievable performance ever. The design parameter, ρ_1, required by our algorithm was $\rho_1 = 4$, and ρ_0 which must be sufficiently high was set to $\rho_0 = 8000$. Moreover, we fix $\delta_{\bar{\tau}} = 0.2/B$ and $\delta_{\bar{\tau}} = 0.2^{\circ}$. It was also found that $R_1 = R_2 = 1000$ generated realizations (during "STAGE I" and "STAGE II") provide sufficiently accurate IS-based MLEs for both the TDs and AoAs as will be seen from the subsequent simulations.

We begin by simulating the two estimators in a relatively *comfortable* situation where the paths are widely separated both in time and space. The results are shown in Fig. 8 for two equi-powered paths that are located at directions $\bar{\alpha}_1 = 20^{\circ}$ and $\bar{\alpha}_2 = 45^{\circ}$ with respective delays $\bar{\tau}_1 = 2/B$ and $\bar{\tau}_2 = 5/B$. There it is seen that the proposed IS-based ML estimator (referred to here as "New IS-ML") outperforms UMP in terms of TDs estimation, although the two estimators exhibit almost the same performance in terms of angle estimation over the entire SNR range. Most remarkably, the proposed IS-based ML estimator reaches the CRLB both in terms of delay and angle estimations thereby confirming its statistically efficiency.

We also assess the performance of both estimators in a more challenging scenario where the paths have closely-spaced angles or delays. To do so, we consider in Fig. 9 three paths in a situation where the two paths that have small angular separation are well separated in the delay line and vice versa. More specifically, the paths are located
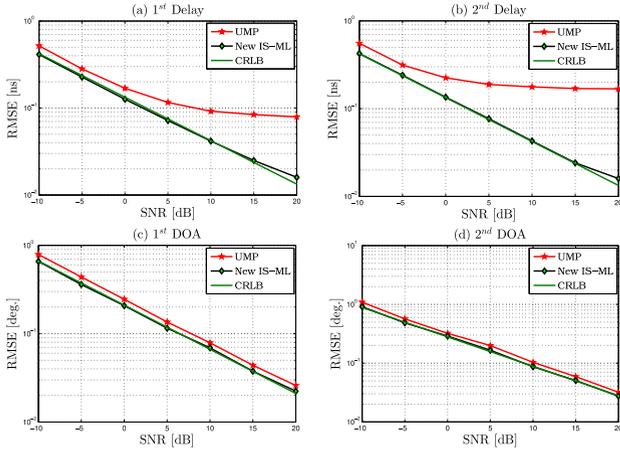
Fig. 8. RMSE for the TDs and AoAs with $M + 1 = 245$ subcarriers, for large angular and delay separations.
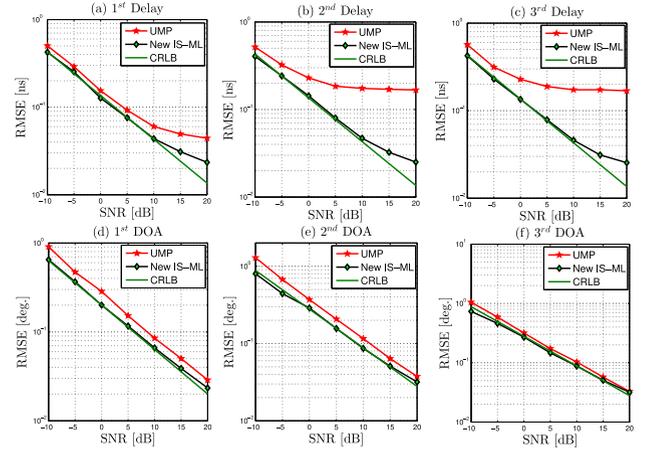

Fig. 9. RMSE for the TDs and AoAs with $M = 245$ subcarriers, for paths with closely-spaced angles and large delay separations and vice versa.

at directions $\bar{\alpha}_1 = 10°$, $\bar{\alpha}_2 = 44.5°$ and $\bar{\alpha}_3 = 45°$ with respective delays $\bar{\tau}_1 = 2/B$, $\bar{\tau}_2 = 3/B$ and $\bar{\tau}_3 = 8/B$. Here again, its seen that the proposed IS-based ML estimator exhibits a huge performance advantage in terms of delays estimation as compared to UMP.

10.2.2 Localization with Real-World Measurments

Here, we evaluate the localization performance of the proposed algorithm using real-world measurements in the form of measured channel frequency responses (CFRs) that were obtained in [13] using the IEEE 802.11ac standard's setup parameters. In the tested scenario, a multilateral localization system is considered wherein a mobile unit (MU) broadcasts a reference/known signal to a number of access points (APs). Each AP forwards the recorded observations to a central unit (CU). The latter extracts the required CFR measurements (corresponding to each AP) and then feeds them to the new IS-based ML JADE technique which is itself executed locally at the CU. The obtained IS-based AoA and TDOA estimates from all APs are then blended together to find the physical location of the MU. If the need be, the computed coordinates can be fed back to the MU from the central unit. According to the measurement setup depicted in [13, Fig. 5], the APs (denoted as AP1, AP2, AP3, and AP4) and the MU were positioned at $(146.2, -172.6)$ cm, $(841.6, -213.2)$ cm, $(907.7, 338.2)$ cm, $(19.1, 333.4)$ cm, and $(462.1, 161.4)$ cm, respectively. It is worth mentioning here that two of the APs have no line of sight (LOS) component to the MU. Moreover, as explained in [13], 310 different channel measurements were collected over a bandwidth of $B = 80$ MHz using the Agilent ENA E5071C network analyzer and a uniform linear array of six antennas at each AP, all configured according to the IEEE 802.11ac standard's setup parameters.

To localize the MU, we consider the hybrid Time Difference of Arrival (TDOA) and AoA localization technique proposed in [13, Section IIV] with the TDOA being time difference of arrival between each AP and a reference AP (here chosen to be AP1). Indeed, it was shown that the hybrid TDOA and AoA localization procedure outperforms the procedures that are based on either AoA or TDOA only. This hybrid localization approach, however, requires the knowledge of the covariance matrix $\mathbf{Q}$ of all the estimated angles and delays in order to reduce the effect of outlier AoA or TDOA estimates. In [13], $\mathbf{Q}$ was obtained from the

different estimates corresponding to the different 310 channel measurements. In the sequel, we shall refer to this procedure as the covariance-based localization technique. It should be emphasized, however, that this is a somewhat non practical solution since the MU needs to be localized using a single set of channel measurements. In this situation, one can use the same hybrid localization procedure by simply setting $\mathbf{Q} = \mathbf{I}$ which is referred to hereafter as the covariance-free procedure in the sequel. If the underlying JADE algorithm is already outlier free, then the more practical covariance-free method will also be accurate.

Fig. 10 depicts the location estimates obtained from the TDOA and AoA estimates returned by both UMP and the proposed IS-based ML estimator. By inspecting Figs. 10a and 10c, it is seen that both UMP and the new IS-ML algorithms yield accurate location estimates when used in conjunction with the covariance-based localization procedure. Indeed, all the corresponding location estimates are scattered in the close vicinity of the true MU position. A distinct advantage for the proposed IS-ML algorithm over UMP is, however, observed when the more practical covariance-free localization procedure is used (i.e., using a single channel measurement). In fact, as seen from Figs. 10b and 10d, while all IS-based estimated locations remain very close to the true MU position, UMP exhibits many outlier locations which are roughly 80 and 30 cm away from the MU along the x- and y-axes, respectively. This is mainly due to some inaccurate TDOA and AoA estimates for UMP.

For better illustration, we plot in Fig. 11 the empirical complementary distribution function (CDF) of the position error

$$ e_z = \sqrt{(\hat{x} - x)^2 + (\hat{y} - y)^2}, \tag{78} $$

where (x, y) and $(\hat{x}, \hat{y})$ are the true coordinates of the MU and their estimates, respectively.

As seen from Fig. 11a, both UMP and IS ML techniques yield remarkably small localization errors which are smaller than 10 cm at all times, when used with the covariance-based localization procedure. Fig. 11b depicts the CDF when the more practical covariance-free localization procedure is applied using the TDOA and AoA estimates provided by each algorithm. There, its is seen that IS-ML still provides a localization error smaller than 10 cm in 90 percent of the cases (and never exceed 15 cm) while UMP localization errors are higher than 70 cm in 10 percent of the cases.
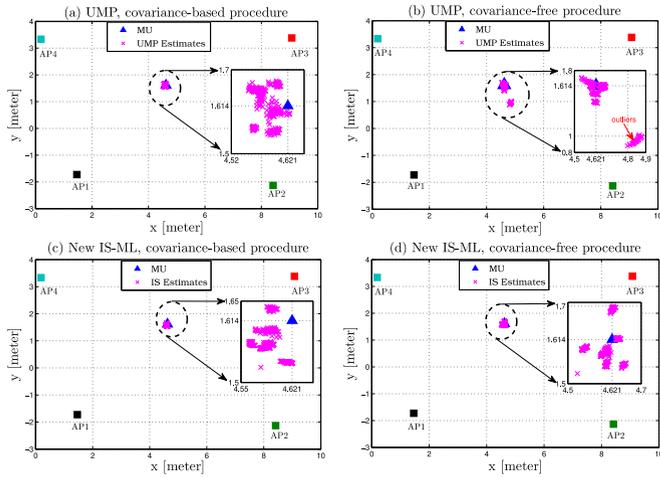
Fig. 10. Constellation of the location estimates in the XY plane for: (a) UMP with weighting matrix, (b) UMP without weighting matrix, (c) IS ML with weighting matrix, and (d) IS ML without weighting matrix.
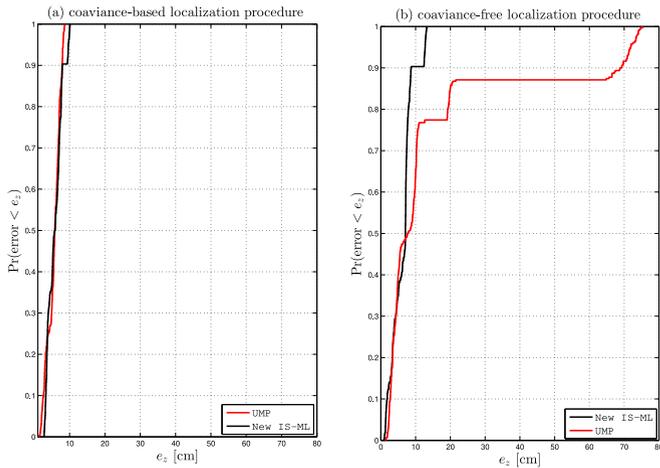

Fig. 11. CDF of the position error e_z for both IS-ML and UMP: (a) Covariance-based localization procedure and (b) covariance-free localization procedure.

10.3 AoA and TD Estimation Accuracies: Single-Carrier Case

In what follows, we will compare our new IS-based ML estimator to the most known JADE techniques that were developed for single-carrier systems. Specifically, we consider the two most powerful subspace-based methods, namely, TST-MUSIC [18] and SI-JADE [20] along with the only two existing ML-type methods which are IML [21] and SAGE [22]. All the estimators are also gauged against the CRLB [20] as an overall benchmark that reflects, for every considered setup, the best achievable performance ever. In all subsequent simulations, we consider a ULA consisting of $P = 5$ receiving antenna elements with half-wavelength spacing, and $M = 128$ received samples. Moreover, as a fast visual reminder, subspace-based and ML techniques are plotted with dashed and solid lines, respectively.

As done for the multicarrier case, we begin by simulating all the estimators in a relatively *comfortable* situation where the paths are widely separated both in time and space. The results are shown in Fig. 12 for a linear chirp signal that is sampled at its Nyquist rate and we consider—as representative example—two equi-powered paths that are located at
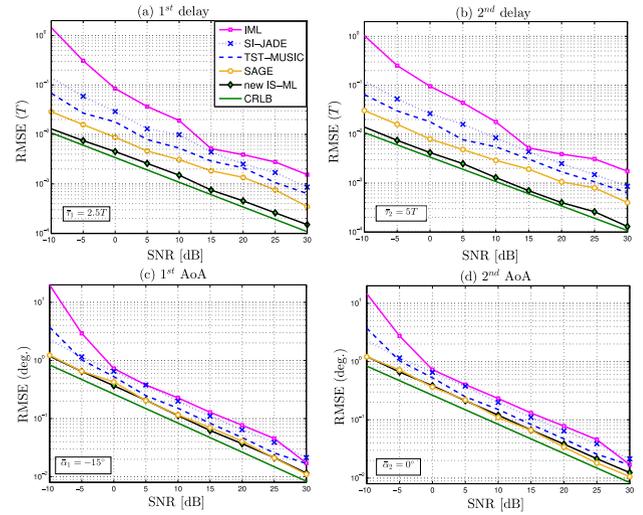

Fig. 12. RMSE for the TDs and AoAs with $M = 128$ samples for *large* angular and delay separations.
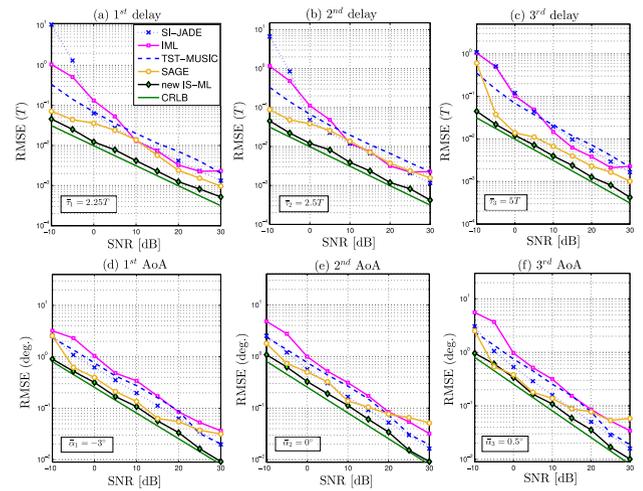

Fig. 13. RMSE for the TDs and AoAs with $M = 128$ samples for paths with closely-spaced angles and large delay separations and vice versa.

directions $\bar{\alpha}_1 = -15°$ and $\bar{\alpha}_2 = 0°$ with respective delays $\bar{\tau}_1 = 2.5\,T$ and $\bar{\tau}_2 = 5\,T$ wherein $T = T_s$.

For such large angle/delay separations, ML-type SAGE offers an AoA estimation performance as superior as ours, at the cost, however, of about 13 times higher complexity as will be shown at the end of this section. The other ML-type solution (i.e., IML), on the other hand, is severely affected in performance at lower SNR values due to noise amplification since it requires the division of the frequency-domain received signal by $s(\omega_m)$. To circumvent this problem, it was suggested in [21] that only the frequency bins $\{\omega_m\}_m$ for which $\{|s(\omega_m)|^2\}_m$ are significantly greater than the noise power σ^2 be used. Typically, the authors impose a threshold of 30 dB, i.e., only the frequency-domain observations, $\{\mathbf{x}(\omega_m)\}_{m'}$ for which $10\log_{10}(|s(\omega_m)|^2/\sigma^2) \geq 30$ dB are exploited during the estimation process. Obviously, as the SNR decreases (i.e., σ^2 increases), the number of useful observations decreases affecting thereby the overall performance of IML.

In the following, the known transmitted signal is a block of $K = 64$ BPSK symbols—each of period T—that are pulse-shaped with a raised-cosine filter of *excess* bandwidth $\Delta f = 0.3$. In this case, $T_s = T/2$ is the largest sampling period

TABLE 1
Complexity Assessment of the Considered JADE Algorithms (cf. Table 2)

Algorithm	Complexity	Complexity ratio
IS-ML	$(P+1)M\log(M) + (G_1+G_2)PM + (G_1+G_2)P(K_1+K_2) + 2\big[(K_1+K_2)+M\big] + (G_2+1)^2 + Q\big[(K_2+1)^2+6\big] + 3R\big[2(MPQ+Q^2)+Q^3\big] + 12R$	1.00
SAGE	$\big[(2PM+2P+1)K + Q(M(2P+1))(G+1) + 2Q\big]Q + \bar{N}_{\text{iter}}^{\text{SAGE}}Q\big[2(Q+1)P + 2(Q+3)(P+M) + Q + K + M(2P+1)(K+2+G) + Q+2\big]$	12.19
IML	$(P+1)M\log(M) + Q\big[((2P+P^2) + M(Q+P+P^2+1) + (P^3+P))K + \bar{N}_{\text{iter}}^{\text{IML}}(M(G+2PQ^2+Q^3+2QP+Q+2+Q^2)+Q^3+PQ^3+2PK)\big]$	2.99
TST-MUSIC	$N_{\text{S-MUSIC}}\big[N_{\text{burst}}P^2 M_{\text{burst}} + P^3 + (P+P^3)K + P^3 M_{\text{burst}}\big] + N_{\text{T-MUSIC}}\big[N_{\text{burst}}M_{\text{burst}}^2 P + M_{\text{burst}}^3 + (M_{\text{burst}}^2 + M_{\text{burst}})G + PM_{\text{burst}}^3\big].$	22.40
SI-JADE	$(P+1)M\log(M) + \big[P_1 m_2 + (m_1 P_1 m_2(M-m_1+1))\big]m_2 m_1 + m_2(M-m_1+1)(2m_1 P_1^2 + 4m_1 P_1)4N_{\text{row}}^2 N_{\text{col}} + 2N_{\text{col}}^3 + 4(m_1 P_1)^2 Q + 7Q^3$	3.29
UMP	$(WU)^2(P-W+1)(M-U+1) + 17W^3U^3/3 + 2W^2U^2(P-W+1)(M-U+1) + 8/3Q^3 + 2Q^2(2WU-W-U) + 17Q^3$	1.15

that verifies the Nyquist rate for all the excess bandwidth values (or roll-off factors). We then assess the performance of all the estimators in a more challenging scenario where the paths have closely-spaced angles or delays. To do so, we consider in Fig. 13 three paths in a situation where the two paths that have small angular separation are well separated in the delay line and vice versa. More specifically, the paths are located at directions $\bar{\alpha}_1 = -3°$, $\bar{\alpha}_2 = 0°$ and $\bar{\alpha}_3 = 0.5°$ with respective delays $\bar{\tau}_1 = 2.25\,T$, $\bar{\tau}_2 = 2.5\,T$ and $\bar{\tau}_3 = 5\,T$.

It is seen that the behavior of TST-MUSIC remains almost unchanged compared to the *comfortable* situation of Fig. 12. This is hardly surprising since TST-MUSIC was designed specifically for such type of situations [18]. In fact, it applies the traditional MUSIC algorithm several times by alternating between temporal and spatial spectral estimations in order to use the angular (resp. delay) separation to resolve multipath components that are closely spaced in the delay (resp. angular) domain. The performance of SI-JADE, however, deteriorate at low SNR levels. The improvements of IML in terms of AoA estimation as compared to Fig. 12 (at low SNR values) is due to the improved spectral content, $s(\omega)$, of the RRC waveform as compared to the chirp signal of Fig. 12. In contrast, our new IS-based estimator is oblivious to the shape of the transmitted waveform and continues to achieve the CRLB over the entire SNR range.

10.4 Complexity Assessment

In Table 1, we computed the total number of operations (i.e., $+, \times, \div$) required by each technique. Please refer to Table 2 for the definition of the various parameters. For SAGE and IML, which are iterative in nature, we computed the average number of iterations, $\bar{N}_{\text{iter}}^{\text{SAGE}}$ and $\bar{N}_{\text{iter}}^{\text{IML}}$, they took until convergence by means of Monte-Carlo simulations at a fixed SNR = 0 dB. Then, $\bar{N}_{\text{iter}}^{\text{SAGE}}$ and $\bar{N}_{\text{iter}}^{\text{IML}}$ are used as multiplicative factors to their complexities measured over a single iteration. For the sake of clarity, we introduced $P_1 = m_1(P-m_2+1)$, $N_{\text{row}} = m_1(P-m_2+1)$, and $N_{\text{col}} =$

TABLE 2
Definition of the Complexity Analysis Parameters in Table 1

Parameter	Description
K_1, G_1, K_2, G_2	Number of grid points for IS-ML
R	Number of generated realizations for IS-ML
$N_{\text{burst}}, M_{\text{burst}}$	Number and size of the data bursts for TST-MUSIC
$N_{\text{S-MUSIC}}, N_{\text{T-MUSIC}}$	Number of MUSIC blocks in the space and time domains
$\bar{N}_{\text{iter}}^{\text{SAGE}}$	Number of iterations for IML
$\bar{N}_{\text{iter}}^{\text{SAGE}}$	Number of iterations for SAGE
K, G	Number of grid points for IML and SAGE
m_1, m_2	Stacking parameters for SI-JADE
U, W	Pencil parameters for UMP

$2m_2(M-m_1+2)$. The results in Table 1 were obtained by fixing the number of generated realizations required by the proposed IS-ML JADE to $R = 1000$ as was the case in all experiments discussed in the simulations section. The number of samples and antenna elements were set to $M = 128$ and $P = 5$, respectively.

We see from Table 1 that the new IS-based ML JADE estimator exhibits remarkable computational savings compared to TST-MUSIC and the two existing ML estimators. For instance, with the simulation setup considered in Fig. 12 (i.e., $P = 5$, $M = 128$, and $\bar{Q} = 2$), IML, SAGE, and TST-MUSIC are, respectively, 3, 12, and 22 times more complex than IS-ML.

11 CONCLUSION

In this paper, we proposed a new non-iterative and statistically efficient ML solution for the joint estimation of the time delays and angles-of-arrival of overlapping reflections of a signal with a known waveform. Based on the importance sampling concept, this new ML JADE technique applies to both single- and multi-carrier models and enjoys guaranteed global optimality with super-resolution capabilities. Typically, it is able to resolve multipath components with simultaneous angle and delay separations as low as $\Delta\bar{\alpha} = 0.5°$ and $\Delta\bar{\tau} = 0.25\,T$ while achieving the CRLB even at SNR levels as low as -10 dB. By exploiting the sparsity feature of a pseudo-pdf that is *intrinsic* to the new algorithm, we also proposed a new approach that can accurately estimate the unknown number of paths. Computer simulation results show the clear superiority of the new IS-based ML estimator over state-of-the-art JADE techniques both in accuracy and complexity. Simulations with real channel measurements in an indoor an environment also show the high accuracy of the IS-based ML JADE technique in real-world localization applications.

REFERENCES

[1] F. Bellili, S. Ben Amor, S. Affes, and A. Samet, "A new importance-sampling ML estimator of time delays and angles of arrival in multipath environments," in *Proc. IEEE Int. Conf. Acoust. Speech Signal Process.*, 2014, pp. 4219–4223.
[2] A. J. Van der Veen, "Algebraic methods for deterministic blind beamforming," *Proc. IEEE*, vol. 86, no. 10, pp. 1987–2008, Oct. 1998.
[3] J. T. Chen and Y. C. Wang, "Performance analysis of the parametric channel estimators for MLSE equalization in multipath channels with AWGN," *IEEE Trans. Commun.*, vol. 49, no. 3, pp. 393–396, Mar. 2001.

[4] B. R. Phelan, E. H. Lenzing, and R. M. Narayanan, "Source localization using unique characterizations of multipath propagation in an urban environment," in *Proc. IEEE Sensor Array Multichannel Signal Process. Workshop*, 2012, pp. 189–192.

[5] M. Z. Rahman and L. Kleeman, "Paired measurement localization: A robust approach for wireless localization," *IEEE Trans. Mobile Comput.*, vol. 8, no. 8, pp. 1087–1102, Aug. 2009.

[6] S. A. Golden and S. S. Bateman, "Sensor measurements for WiFi location with emphasis on time-of-arrival ranging," *IEEE Trans. Mobile Comput.*, vol. 6, no. 10, pp. 1185–1198, Oct. 2007.

[7] C. Nerguizian, C. Despins, and S. Affes, "Geolocation in mines with an impulse response fingerprinting technique and neural networks," *IEEE Trans. Wireless Commun.*, vol. 5, no. 3, pp. 603–611, Mar. 2006.

[8] C. Nerguizian, C. Despins, and S. Affes, "Method and system for indoor geolocation using an impulse response fingerprinting technique," U.S. Patent 7 630 943 B2, Dec. 8, 2009.

[9] A. Jaffe and M. Wax, "Single-site localization via maximum discrimination multipath fingerprinting," *IEEE Trans. Signal Process.*, vol. 62, no. 7, pp. 1718–1728, Apr. 2014.

[10] C. Feng, W. S. A. Au, S. Valaee, and Z. Tan, "Received-signal-strength-based indoor positioning using compressive sensing," *IEEE Trans. Mobile Comput.*, vol. 11, no. 12, pp. 1983–1993, Dec. 2012.

[11] S. Yoon, K. Lee, Y. Yun, and I. Rhee, "ACMI: FM-Based indoor localization via autonomous fingerprinting," *IEEE Trans. Mobile Comput.*, vol. 15, no. 6, pp. 1318–1332, Jun. 2016.

[12] A. Gaber and A. Omar "A study of wireless indoor positioning based on joint TDOA and DOA estimation using 2-D matrix pencil algorithms and IEEE 802.11ac," *IEEE Trans. Wireless Commun.*, vol. 14, no. 5, pp. 2440–2454, May 2015.

[13] A. Gaber and A. Omar, "Utilization of multiple-antenna multicarrier systems and NLOS mitigation for accurate wireless indoor positioning," *IEEE Trans. Wireless Commun.*, vol. 15, no. 10, pp. 6570–6584, Oct. 2016.

[14] N. Yilmazer, S. Ari, and T. K. Sarkar, "Multiple snapshot direction data domain approach and ESPRIT method for direction of arrival estimation," *Digit. Signal Process.*, vol. 18, no. 4, pp. 561–567, Jul. 2008.

[15] H. Wang, S. Kay, and S. Saha, "An importance sampling maximum likelihood direction of arrival estimator," *IEEE Trans. Signal Process.*, vol. 56, no. 10, pp. 5082–5092, Oct. 2008.

[16] A. Gaber and A. Omar, "A study of TDOA estimation using Matrix Pencil algorithms and IEEE 802.11ac," in *Proc. Ubiquitous Positioning Indoor Navigation Location Based Service*, Oct. 2012, pp. 1–8.

[17] A. Masmoudi, F. Bellili, S. Affes, and A. Stéphenne, "A maximum likelihood time delay estimator in a multipath environment using importance sampling," *IEEE Trans. Signal Process.*, vol. 61, no. 1, pp. 182–193, Jan. 2013.

[18] Y. Wang, J. Chen, and W. Fang, "TST-MUSIC for joint DOA-delay estimation," *IEEE Trans. Signal Process.*, vol. 49, no. 4, pp. 721–729, Apr. 2001.

[19] M. Vanderveen, A. Vanderveen, and A. Paulraj, "Estimation of multipath parameters in wireless communications," *IEEE Trans. Signal Process.*, vol. 46, no. 3, pp. 682–690, Mar. 1998.

[20] M. Vanderveen, A. Vanderveen, and A. Paulraj, "Joint angle and delay estimation using shift-invariance techniques," *IEEE Trans. Signal Process.*, vol. 46, no. 2, pp. 405–418, Feb. 1998.

[21] M. Wax and A. Leshem, "Joint estimation of time delays and directions of arrival of multiple reflections of a known signal," *IEEE Trans. Signal Process.*, vol. 45, no. 10, pp. 2477–2477, Oct. 1997.

[22] B. H. Fleury, M. Tschudin, R. Heddergott, D. Dahlhaus, and I. K. Pedersen, "Channel parameter estimation in mobile radio environments using the sage algorithm," *IEEE J. Sel. Areas Commun.*, vol. 17, no. 3, pp. 434–450, Mar. 1999.

[23] M. Pincus "A closed form solution for certain programming problems," *Operations Res.*, vol. 16, pp. 690–694, 1962.

[24] R. Y. Rubinstein and D. P. Kroese, *Simulation and the Monte Carlo Method*. Hoboken, NJ, USA: Wiley, 2009.

[25] S. Kay and S. Saha, "Mean likelihood frequency estimation," *IEEE Trans. Signal Process.*, vol. 48, no. 7, pp. 1937–1946, Jul. 2000.

[26] S. Saha and S. M. Kay, "Maximum likelihood parameter estimation of superimposed chirps using Monte Carlo importance sampling," *IEEE Trans. Signal Process.*, vol. 58, no. 2, pp. 224–230, Feb. 2002.

[27] H. Wang and S. Kay, "Maximum likelihood angle-doppler estimator using importance sampling," *IEEE Trans. Aerosp. Electron. Syst.*, vol. 46, no. 2, pp. 610–622, Apr. 2010.

[28] J. Chen, Y. C. Wu, S. C. Chan, and T. S. Ng, "Joint maximum-likelihood CFO and channel estimation for OFDMA uplink using importance sampling," *IEEE Trans. Veh. Technol.*, vol. 57, no. 6, pp. 3462–3470, Nov. 2008.

[29] J. Chen, Y. C. Wu, S. Ma, and T. S. Ng, "Joint CFO and channel estimation for multiuser MIMO-OFDM systems with optimal training sequences," *IEEE Trans. Signal Process.*, vol. 56, no. 8, pp. 4008–4019, Aug. 2008.

[30] G. Wang and H. Chen, "An importance sampling method for TDOA-based source localization," *IEEE Trans. Wireless Commun.*, vol. 10, no. 5, pp. 1560–1568, May 2011.

[31] A. Masmoudi, F. Bellili, S. Affes, and A. Stéphenne, "A non-data-aided maximum likelihood time delay estimator using importance sampling," *IEEE Trans. Signal Process.*, vol. 59, no. 10, pp. 4505–4515, Oct. 2011.

[32] A. Gaber, *Wireless Indoor Positioning based on TDOA and DOA Estimation Techniques using IEEE 802.11 Standards*, PhD Thesis, Faculty Electr. Eng. Inf. Technol., Otto von Guericke Univ. Magdeburg, Magdeburg, Germany, pp. 1–239, May 2015. Available. [Online]: https://d-nb.info/1072146673/34

[33] P. Stoica and A. Nehorai, "On the concentrated stochastic likelihood function in array signal processing," *Circuits Syst. Signal Process.*, vol. 14, pp. 669–674, Sep. 1995.

[34] H. Golub and V. Pereyra, "The differentiation of pseudo-inverses and non-linear least squares problems whose variables separate," *SIAM J. Numerical Anal.*, vol. 10, no. 2, pp. 413–432, Apr. 1973.

[35] S. M. Kay, *Intuitive Probability and Random Processes using MATLAB*. Berlin, Germany: Springer, 2005.

[36] M. Wax and T. Kailath, "Detection of signals by information theoretic criteria," *IEEE Trans. Acoust. Speech Signal Process.*, vol. 33, no. 2, pp. 387–392, Apr. 1985.

[37] S. Kay, "Comments on frequency estimation by linear prediction," *IEEE Trans. Acoust. Speech Signal Process.*, vol. 27, no. 2, pp. 198–199, Apr. 1979.

[38] M. Evans and T. Swartz, *Approximating Integrals via Monte Carlo and Deterministic Methods*. New York, NY, USA: Oxford Univ. Press, 2000.

[39] K. V. Mardia, *Statistics of Directional Data*. New York, NY, USA: Academic, 1972.

[40] S. M. Kay, *Fundamentals of Statistical Signal Processing: Vol. 1—Estimation Theory*. Englewood Cliffs, NJ, USA: Prentice Hall, 1993.

[41] M. Wax and T. Kailath, "Detection of signals by information theoretic criteria," *IEEE Trans. Acoust. Speech Signal Process.*, vol. ASSP-33, no. 2, pp. 387–392, Apr. 1985.

Faouzi Bellili received the BEng degree (with Hons.) in electrical engineering from Tunisia Polytechnic School, in 2007, the MSc and PhD degrees (both with the highest honors) from the National Institute of Scientific Research (INRS-EMT), University of Quebec, Montreal, QC, Canada, in 2009 and 2014, respectively. From Sept. 2014 to Sept. 2016, he was working as a Research Associate with INRS-EMT where he coordinated a major multi-institutional NSERC Collaborative R&D (CRD) project on 5th-Generation (5G) Wireless Access Virtualization Enabling Schemes (5G-WAVES). From Dec. 2016 to May 2018, he was a postdoctoral fellow with the University of Toronto, ON, Canada. Currently, he is an assistant professor with the Department of Electrical and Computer Engineering, University of Manitoba, Winnipeg, MB, Canada. His research focuses on statistical and array signal processing for wireless communications and 5G-enabling technologies. Dr. Bellili was awarded the very prestigious NSERC PDF Grant over the period 2017-2018. He was also awarded another prestigious PDF Scholarship offered over the same period (but declined) from the "Fonds de Recherche du Québec Nature et Technologies" (FRQNT). He was also awarded the INRS Innovation Award for the year 2014/2015, the very prestigious Academic Gold Medal of the Governor General of Canada for the year 2009-2010, and the Excellence Grant of the Director General of INRS for the year 2009-2010. He received the Award of the best MSc Thesis in INRS-EMT for the year 2009-2010 and twice – for both the MSc and PhD programs – the National Grant of Excellence from the Tunisian Government. In 2011, he was also awarded the Merit Scholarship for Foreign Students from the Ministère de l'Éducation, du Loisir et du Sport (MELS) of Québec, Canada. Dr. Bellili serves regularly as a TPC member for major IEEE conferences and acts as a reviewer for many international scientific journals and conferences.

Souheib Ben Amor received the diplôme d'Ingénieur in telecommunications from the National Engineering School of Tunis, in 2013 and the MSc degree from the Institut National de la Recherche Scientifique-Énergie, Matériaux, et Télécommunications (INRS-ÉMT), Université du Québec, Montréal, QC, Canada, in 2016. He is currently working toward the PhD degree at INRS-ÉMT. He held an internship at Ericsson Canada in the winter of 2015 as part of the create-PERSWADE training program. He was also a research intern at Interdigital Canada in the summer of 2015. His PhD program is in the field of statistical signal processing and array processing and their applications to wireless communications. He received a scholarship for MSc studies under the agreement between the Tunisian Government and INRS. He also received the INRS scholarship for his PhD studies.

Sofiène Affes (S'94-SM'04) received the diplôme d'Ingénieur in telecommunications and the PhD degree (Hons.) in signal processing from the École Nationale Supérieure des Télécommunications, Paris, France, in 1992 and 1995, respectively. He was a research associate with INRS, Montreal, QC, Canada, until 1997, an assistant professor until 2000, and an associate professor until 2009. He is currently a full professor and director of PERSWADE, a unique U.S. $4M research training program on wireless in Canada involving 27 faculty members from eight universities and 10 industrial partners. From 2003 to 2013, he was a Canada research chair in wireless communications. He has been a recipient of a Discovery Accelerator Supplement Award twice from NSERC, from 2008 to 2011 and from 2013 to 2016. He is an associate editor for the *IEEE Transactions on Communications* and the *Journal on Wireless Communications and Mobile Computing* (Wiley). He was previously an associate editor of the *IEEE Transactions on Wireless Communications* and the *IEEE Transactions on Signal Processing*. He already served as a general co-chair of the IEEE VTC'2006-Fall and the IEEE ICUWB 2015, both held in Montreal, QC, Canada. For his contributions to the success of both events, he received a Recognition Award from the IEEE Vehicular Technology Society in 2008 and a Certificate of Recognition from the IEEE Microwave Theory and Techniques Society in 2015. He also served as the general chair of 28th IEEE PIMRC which was held in Montreal in the fall 2017. He is a senior member of the IEEE.

Ali Ghrayeb received the PhD degree in electrical engineering from the University of Arizona, Tucson, in 2000. He is currently a professor with the Department of Electrical and Computer Engineering, Texas A&M University at Qatar. Prior to his current position, he was a professor in the electrical and computer engineering with Concordia University, Montreal, Canada. He is a co-recipient of the IEEE Globecom 2010 Best Paper Award. He is the coauthor of the book *Coding for MIMO Communication Systems* (Wiley, 2008). His research interests include wireless and mobile communications, physical layer security, massive MIMO, wireless cooperative networks, and cellular networks. He served as an instructor or co-instructor in technical tutorials at several major IEEE conferences. He served as the executive chair of the 2016 IEEE WCNC conference, and as the TPC chair/co-chair of several symposia of major IEEE conferences. He has served on the editorial board of several IEEE and non-IEEE journals. He is a senior member of the IEEE.

▷ **For more information on this or any other computing topic, please visit our Digital Library at** www.computer.org/publications/dlib.